Doctoral Dissertation

博士論文

Characterization of *Dclk1* isoforms in the developing mouse brain

(マウス大脳皮質発生における*Dclk1*スプライシングアイソフォームの解析)

Dissertation Submitted for the Degree of Doctor of Philosophy

December 2020

令和2年12月博士(理学)申請

Department of Biological Sciences, Graduate School of Science,

The University of Tokyo

東京大学大学院理学系研究科生物科学専攻

BERGOGLIO Emilia

ベルゴリオ　エミリア

TABLE OF CONTENTS

TABLE OF FIGURES

ABSTRACT

Doublecortin-like kinase 1 (DCLK1) is a Doublecortin family kinase involved in a range of brain development processes including cell migration, axon/dendrite growth, and synapse development. The *Dclk1* gene potentially generates multiple splicing isoforms, but the detailed expression patterns in the brain as well as *in vivo* functions of each isoform are still incompletely understood. Here I assessed expression patterns of DCLK1 isoforms using multiple platforms including *in silico*, *in situ*, *in vivo,* and *in vitro* datasets in the developing mouse brain, and show quantitative evidence that among the four DCLK1 isoforms, DCLK1-L and DCL are mainly expressed in the embryonic cortex whereas DCLK1-L and CGP16 become dominant compared to DCL and CARP in the postnatal cortex. I also provide compelling evidence that DCLK1 isoforms are distributed in the partially distinct brain regions in the embryonic and the postnatal stages. I further show that overexpression of DCLK1-L, but not the other isoforms, in neural progenitors causes severe migration defects in the cortex, and that the migration defects are dependent on the kinase activity of DCLK1-L. My data thus uncovers partially segregated localization of DCLK1 isoforms in the developing mouse brain and suggest different roles for distinct DCLK1 isoforms in the brain development and function.

INTRODUCTION

The *Dclk1* gene and its variants

DCLK1 encodes for a protein kinase belonging to the doublecortin (*DCX*) family of microtubule associated proteins (MAPs). *DCLK1* shows the highest reported homology with the X-linked *DCX*, which, in humans, was originally identified as the causative gene for lissencephaly in males as well as subcortical band heterotopia (or doublecortex) in females (Gleeson et al., 1998; Des Portes et al., 1998). In mice, *Dclk1* presents 20 exons and undergoes complex alternative splicing, with two distinct promoters (a 5' promoter before exon 1, and a 3' promoter before exon 6), giving rise to a total of twelve known variants (Table 1). In turn, these variants can be grouped in four different isoform categories according to their domains (Fig. 1; Table 1): DCLK1-Long (DCLK1-L), Doublecortin-like (DCL), Candidate plasticity gene 16 (CPG16), and Ca^{2+}/calmodulin-dependent protein kinase-related peptide (CARP). Specifically, the 5' promoter gives rise to the classic isoform, DCLK1-L, which is characterized structure-wise by a tandem of MT-binding domains at the N-term, a linker PEST domain, which is rich in Ser/Pro residues and is thought to be involved in binding other proteins (Nagamine et al., 2011), and a Ser/Thr protein kinase domain at the C-term. DCL, so-called because it shares 70% homology with *DCX*, only possesses the MT-binding domain, and is also originated by the 5' promoter. The 3' promoter gives rise to shorter isoforms of CPG16, which only presents the kinase domain, and the even shorter CARP.

The pattern of expression of these different isoforms varies depending on developmental time: the current understanding is that, in the murine brain, DCLK1-L and DCL are predominantly expressed in the embryonic brain and in neuronal populations that also express DCX (Omori et al., 1998), such as newly generated, radially migrating neurons, and there is evidence of DCLK1-L expression in progenitors, differently from DCX (Shu et al., 2006). However, DCLK1-L expression is still detectable postnatally, and albeit declining with the development, expression can be observed in the adult brain (Shin et al., 2013; Koizumi et al., 2017; Zygmunt et al., 2018). On the other hand, CPG16 and CARP have been less studied, and their expression pattern has only recently been investigated. Current data suggests they are predominantly expressed postnatally (Burgess and Reiner, 2002; Engels et al., 2004).

Functionally speaking, the proteins belonging to the *Dcx* family are known for their multiple roles in various stages of neural circuit formation including dendritic growth and spine formation, as well as neuronal migration and axon outgrowth through its microtubule binding affinity (Gleeson et al., 1999; Francis et al., 1999; Tanaka et al, 2006; Schaar et al., 2004; Bielas et al., 2007). More specifically, DCLK1-L functions in redundancy with DCX in neuronal migration and axon elongation in the cortex and hippocampus, with an effect which is dosage-dependent (Tanaka et al., 2006; Koizumi et al., 2006; Deuel et al., 2006). In dissociated cortical culture, DCLK1-L is intracellularly localized at the growth cone and in the cell soma (Burgess and Reiner, 2000), partially colocalizes with tubulin while also participating in microtubule polymerization (Lin et al., 2000), and is also enriched in the dendritic compartment of hippocampal neurons (Shin et al., 2013). On the other hand, DCL appears to act in synergy with DCLK1-L and DCX

embryonically (Koizumi et al., 2006; Deuel et al., 2006). However, unlike these two proteins, histochemical studies (Vreugdenhil et al., 2007) indicated that DCL expression is immediately suppressed in the late embryonic stages (E12-17) and is later only expressed in the adult brain in staminal niches such as the dentate gyrus in the hippocampus and the SVZ, and therefore in the rostral migratory stream and olfactory bulb as well (Boekhoorn et al., 2008; Saaltink et al., 2012). DCL is also implicated in a variety of roles in corticogenesis, including regulating the mitotic spindle stability and length, as well neuronal precursors proliferation, at a time point when expression of DCX is largely absent (Vreugdenhil et al., 2007). *Dcx* and *Dclk1* are also thought to act in cooperation to elongate axons and to permit axons to cross the midline (Deuel et al., 2006; Koizumi et al., 2006). This cooperation has been thoroughly established in mice by double knockout (KO) of *Dclk1* and *Dcx* (Deuel et al., 2006; Koizumi et al., 2006), with different effects being observed. In the cortex, *Dclk1* single KO mice show agenesis of the corpus callosum with DCLK1-L and DCL knocked out, and different dosage-depended defects of the commissural tracts in double knock out with *Dcx*, such as defects in cortical lamination which in turn imply defects in neuronal migration (Koizumi et al., 2006). Another mutant model, targeting exons 9 to 11, and therefore DCLK1-L and CPG16, shows no phenotype unless in combination with *Dcx* KO, which caused severe malformation of the hippocampus, with the complete collapse of the Cornu Ammonis (CA) fields, also in a dosage-dependent manner (Deuel et al., 2006). In addition, a complete KO out of both *Dclk1* and *Dcx* proved lethal (Deuel et al., 2006; Koizumi et al., 2006), underscoring the importance of the roles exerted by the *Dcx* protein family. On the other hand, the precise role and expression of CPG16 and CARP are less understood.

CPG16 was originally identified as a protein kinase involved in kainite-induced long-term potentiation (LTP) in hippocampal neurons (Hevroni et al., 1998), whereas CARP is considered an immediate early gene (Berke et al., 1998), Recently, evidence has emerged suggesting that CARP could be involved in memory consolidation (Schenk et al., 2011), and it has been postulated that CPG16 may be involved in cascades downstream cAMP (Silverman et al., 1999). In addition, over-expression of a constitutively active form of this isoform in mice has been shown to induce an increase in anxiety behavior (Schenk et al., 2010). In humans, DCLK1-L and CPG16 are expressed both embryonically and postnatally (Sossey-Alaoui and Srivastava, 1999), with transcript-specific PCRs suggesting that CPG16 is particularly enriched in regions involved in memory, such as the hippocampus (Le Hellard et al., 2009)

In addition to the presented evidence of the importance in physiology and pathology of the *DCLK1* gene, recent developments and improvements in the mining of data extracted from large cohorts of patients, together with a new focus on endophenotypes (Gottesman and Gould, 2003), has led to the discovery of high incidences markers in the form of Single Nucleotide Polymorphism (SNPs) conserved across multiple cohorts of patients. In particular, Genome-wide Association Studies (GWAS) indicate that SNPs are present in various regions important as regulatory elements of splice variants, and that splice variants and their dysregulation are reportedly relevant in diseases (López-Bigas et al., 2005). To date, SNPs in three major areas of interest have been identified (Fig. 2):

- 5'UTR to intron 3, associated with verbal memory,

- intron 5, especially around the promoter region, and in the proximity of the start codon, associated with IQ and verbal memory,
- the area covering introns 15 to 19, associated with IQ.

More recently, a new set of studies based on several cohorts of patients and the association of single phenotypes with specific SNPs, have underscored the importance of various SNPs in the areas mentioned above, linking them to specific Neurodevelopmental Disorders (NDDs): in particular Attention Deficit – Hyperactive Disorder (ADHD) and schizophrenia for intron 3, and a cross-section of psychiatric disorders for intron 19 – 3' UTR (Fig. 3; Le Hellard et al., 2009; Håvik et al., 2012; Wu et al., 2012). Despite all this, information about the isoform-specific expression patterns in the brain as well as *in vivo* function is still limited, especially when it comes to CPG16 and CARP, partially due to the isoforms sharing a number of exons, which makes it hard to selectively label or manipulate single isoforms.

In this study, I aim to characterize the splicing isoforms of *Dclk1*, namely DCLK1-L, DCL, CPG16, and CARP, in the developing mouse brain. To do so, I took advantage of multiple platforms, including *in silico*, *in vitro*, and *in vivo* datasets. I first examined the developmental dynamics of DCLK1 isoform expression using publicly available transcriptome data, as well as by using Western Blot to determine the temporal pattern of expression in an isoform-specific manner. I then sought to observe the spatial expression pattern of the different isoforms both in the developing and the adult murine brain by *in situ* hybridization studies using probes designed for minimal overlapping between isoforms, which showed segregation of expression. To assess the function of

the isoforms *in vivo*, I then overexpressed each isoform in the embryonic cortex and found isoform-specific defects in neuronal migration. The combination of these different methodologies can help shed a light on the differential roles and the *Dclk1* isoforms in brain development and function.

METHODS

Animals

All animal procedures were approved by the Institutional Safety Committee on Recombinant DNA Experiments and Animal Research Committee of the University of Tokyo. C57BL/6J and ICR mice were purchased from SLC Japan. Pregnant ICR mice were purchased from Japan SLC Inc. Mice were housed in a temperature-controlled room with 12 h light/dark cycle.

Plasmids

The coding sequence of the different isoforms was determined according to the Ensembl genome database project (https://asia.ensembl.org/Mus_musculus/Gene/Summary?g=ENSMUSG00000027797&db=core). The full-length murine DCLK1-L (ENSMUST00000054237.13), DCL (ENSMUST00000167204.7), CPG16 (ENSMUST00000070418.8), and CARP (ENSMUST00000199585.4) isoforms were generated by PCR amplification of P7 mouse whole brain cDNA with KOD -Plus-Neo (Toyobo).

The following primers were used (*EcorI* and *KpnI* digestion sites are underlined), also adding Kozak sequence to the forward primers:

	Forward primer	Reverse primer
DCLK1-L	ATGAATTCGCCACCATGTCCTTCGGCA GAGACATGGAGCTGGA	GCGGTACCAAAGGGCGAGTTAGGGGA GCGAACAGTCTCGGAGGA
DCL	ATGAATTCCGCCACCCATGTCGTTCGG CAGAGATATGGAGTTGGA	CGGGTACCCTTTTACACTGAGTCTCCTA CTGAGTCCAAATCATC
CPG16	GCGAATTCCGCCACCATGTTAGAGCTC ATAGAAGT	GCGGTACCAAAGGGCGAATTGGGGGA GCGAACAGTCTCAGAGGA
CARP	AACCGGTGAATTCCCACCATGTTAGAG CTCATAGAAGTTAATGGAAC	AAGGTACCCACTGAGTCTCCTACTGAGT CCAAATCATCCGACG

Cycling conditions were set as:

1. Pre-denaturation: 94°C, 2 minutes
2. Denaturation: 98°C, 10 seconds
3. Annealing: Tm°C (step-up +0.5°C/cycle), 30 seconds
4. Extension: 68°C, 30 second/Kb

Repeat steps 2-4 5 times

1. Denaturation: 98°C, 10 seconds
2. Annealing: Tm°C, 30 seconds
3. Extension: 68°C, 30 second/Kb

Repeat steps 1-3 15 times

Extension: 68°C 5 minutes

Cool down: 16°C ∞

I then gel purified the amplified fragments, digested them with *EcorI* and *KpnI* (NEB), and subsequently inserted them in pcDNA3.1/myc-6xHis (Invitrogen), cloned in HB101 competent cells (Promega). This allowed me to generate Myc-tagged constructs of each isoform. Each isoform-of-interest-Myc constructs were then amplified again, using the following primers and conditions analogous to the ones above:

	Forward primer	**Reverse primer**
DCLK1-L	AAGGATCCGCCACCATGTCCTTC GGCAGAGACATGGAGC	ATTCCGGACAGATCCTCTTCAGAGATGAG TTTAAAGGGCGAGTTAGGGGAGCGAACA
DCL	AAGGATCCGCCACCATGTCGCTT CGGCAGAGATCATGGAGT	ATTCCGGACAGATCCTCTTCTGAGATGAG TTTTTGTTCGGGCCCAAG
CPG16	AAGGATCCGCCACCATGTTAGAG CTCATAGAAGTTAATGG	TTTCCGGACAGATCCTCTTCAGAGATGAG TTTAAAGGGCGAATTGGGGGAGCG
CARP	AAGGATCCACCACCATGTTAGAG CTCATAGAAGTTAATGGAAC	AATCCGGAAATGATGATGATGATGATGGT CGACGGCGCTATTCAG

After amplification, the fragments were digested with *BamHI* and *BspEI* (digestion sites are underlined) and subcloned into *BamHI* - *BspEI* site of pCAG-T2A-EGFP expression vector (Gift from Kazuya Togashi) to generate pCAG-DCLK1-L-Myc-T2A-EGFP, pCAG-DCL-Myc-T2A-EGFP, pCAG-CPG16-Myc-T2A-EGFP, and pCAG-CARP-Myc-T2A-EGFP. The T2A self-cleaving peptide guarantees the cleaving of the inserted contract into two recombinant proteins, Isoform-Myc and EGFP, which made tracking the transfected cells easy.

To generate a dominant-negative version of DCLK1-L (pCAG-DCLK1-L-D511A-Myc-T2A-EGFP), pCAG-DCLK1-Myc-T2A-EGFP is used as a template and amplified as above with primers:

Forward primer	Reverse primer
GAACATCGTCCACCGTGcTATCAAGCCAGAGAACC	GGTTCTCTGGCTTGATAgCACGGTGGACGATGTTC

The amplified fragment, of 8.2 Kb, was then digested with *DpnI* (50U, NEB) at 37°C for 1 hour. Samples were then transformed into HB101 competent cells plated on LB plates with Kanamycin.

Cell culture

HEK293T were cultured in 6 well plates in Dulbecco's Modified Eagle Medium (Gibco) with 10% FCS (Gibco), penicillin/streptomycin (Gibco), and glutaMAX (Gibco) for 24 hour and then transfected using with the plasmids above using polyethylenimine (PEI) as previously described (Longo et al., 2013). Briefly, cells were washed, and new medium was added. DNA and PEI (1:3 ratio; 1 ug DNA/sample) were mixed in serum-free medium and incubated at room temperature for 15 minutes after energetic vortexing for 10 seconds. The mix was then added to the adherent cells, which were grown at 37°C with 5% CO_2. Cells were harvested 48 hours after transfection and cell lysate analyzed by Western Blot as described below.

Western Blotting

Mice aged E14.5, P0, P7, P15, and P30 were sacrificed by decapitation and their brains dissected in ice cold HBSS (Sigma) whereas HEK293T transfected with the plasmids above were washed in PBS. The cortices were when excised and homogenized in IP buffer containing 50 m*M* Tris pH 7.4, 150 m*M* NaCl, 1 m*M* EDTA, 1% TritonX-100, and containing PhosSTOP (Roche) and Complete Protease Inhibitor cocktail (Roche Diagnostics), whereas cells were collected by cell scraper after being immersed in IP buffer for 20 minutes. Samples were centrifuged 20000*g* at 4°C for 20 min. To assess the total number of proteins in the samples, I performed the BCA protein assay (Thermo Fisher) and diluted the sample in Laemmle buffer to a final quantity of 20 ug per sample in a total of 100 uL.

I then casted SDS-Page gels (12.5%). These gels are made of a top stacking gel (40% acrylamide, 0.5M TrisHCl pH6.8, 10% SDS, 10% APS, TEMED) and a bottom separating gel (40% acrylamide, 1.5M TrisHCl pH8.8, 10% SDS, 10% APS, TEMED). 20 uL of samples were then denatured at 98°C for 2 minutes and loaded in the gels. I ran the gels for 2 hours at 20mA, 300V each. I then transferred the protein samples onto a Immobilon – P PVDF membrane (Merk) using wet transfer in Transfer Buffer with 10% Methanol.

After that, membranes were incubated with rabbit anti-DCLK1 antibody C- term (Abcam, ab31704) and N-term (Koizumi et al., 2006) both at the concentration of 1:2000. HEK cells membranes were blocked as above and incubated in mouse anti-Myc 9E10 clone (Roche; 1:2000 dilution) for two hours. In both cases, secondary antibody

incubation with anti-rabbit horseradish peroxidase-conjugated antibody (Jackson) was performed for 2 hours, and blotting was revealed with SuperSignal West Femto Maximum Sensitivity Substrate (Thermo Fisher) on a ImageQuant™ LAS 4000 (GE Healthcare) machine. Anti-beta-actin (1:2000; Cell Signaling Technology) was used as loading control.

To quantify the expression levels of the different isoforms, gels were analyzed as previously described (Tan and Ng, 2008; Gassmann et al., 2009). Briefly, densities were calculated using the ImageJ Gel Analysis plugin, and the relative density of each band was extracted. Relative densities of samples and loading controls were then used to calculate the normalized densities. For plotting these values, I used a custom Python script generating nested bar graphs. For statistical analysis, one-way Anova was used, with the SEM taken as the error bar for each sample.

RNA-seq and splicing variants expression analysis

In order to assess isoform-specific expression dynamics of *Dclk1* during the murine corticogenesis, I examined publicly available RNA sequencing data of the samples of mouse cerebral cortex in various developmental stages (Yan et al., 2015). In the original study, total RNA was extracted from whole cortices of male C57BL/6 mice at different time points. Yan et al. prepared RNA-Seq libraries using the TruSeq RNA Sample Preparation Kit (Illumina) and Paired Ends (2×101-nt) reads were generated using the Illumina HiSeq 2000. The read depth of this study averaged at 57 million reads per sample, making it suitable for splicing studies. For my application, the raw files were

aligned to the Genome Reference Consortium Mouse Build 38 (mm10) reference genome.

First, I prepared a GTF file, a list of the known annotations of exon-intron structure, using the annotated index downloaded from the HISAT2 (Kim et al., 2019) documentation (available at the address https://cloud.biohpc.swmed.edu/index.php/s/grcm38_snp_tran/download). This particular annotation file contains known SNPs as well as transcripts, making it suitable for splicing variants searches. After downloading, the following command has to be given

```
python hisat2_extract_splice_sites.py name-of-annotation-file.gtf
> splicesites.txt
```

in order to prepare the HISAT2 index by loading the known splice sites available via the annotation file.

I then pulled RNA-Seq data for the cortex at E14.5, P0, P7, P15, and P30 from the NCBI Short Read Archive under accessions (Accession SRP055008) and converted it to FASTQ using the SRA-Toolkit (https://github.com/ncbi/sra-tools). I gave the following commands, from the SRA Toolkit,

```
fastq-dump SRR-file-name.1 --split-files
```

to convert the RNA-seq data, provided in SRA format, into Fastq format, making it suitable for mapping with HISAT2. This command also splits the original file in two and needs to be used when dealing with paired ends RNA-Seq datasets. I repeated the same procedure for every time point and their biological replicates. Before performing the alignment, I merged and averaged the replicates using

```
samtools merge [-nr] [-h inh.sam] <out.bam> <in1.bam> <in2.bam>
[...]
```

Then, giving the command

```
hisat2 -p 8 -t -x genome_snp_tran --known-splicesite-infile
splicesites.txt -1 /SRR-file-name1_1.fastq -2 SRR-file-
name1_2.fastq -S aligned.sam
```

I aligned the files with default conditions, and I generated a SAM file called aligned.sam. Samples were also normalized as described by the edgeR documentation (Robinson et al., 2010) on the Galaxy Project (galaxyproject.org). Normalization is a way to scale raw data to make it comparable across samples, and takes into account factors such as sequencing depth, gene composition, and RNA composition. EdgeR uses the trimmed median of M-values to enable downstream differential expression analysis. Following that, I converted the aligned files from SAM to BAM, using Samtools (Li, 2011).

```
samtools view -Sbh aligned.sam > aligned.bam
```

After that, using the commands below, I sorted the BAM files and indexed them to make them readable for downstream applications.

```
samtools sort aligned.bam -o sorted.bam
samtools index | sorted.bam
```

The “index” command generated the .bam.bai index file necessary for downstream applications.

To create a sashimi plot, I used the ggsashimi script (Garrido-Martin et al., 2018) with the command and options

```
sashimi-plot.py -b sorted.bam -c chr3:55520000-55539068 -g
name.of.annotation.file.gtf -o file.name -F svg
```

Probe preparation for *in situ* hybridization

I designed five probes, 4 targeting *Dclk1* isoforms and one targeting *Dcx* to use as a positive control. Probes were designed to target 800 bases from Exon 1 to 3 (Probe A), 320 bases from Exon 6 (Probe B), 633 bases from Exon 8 (Probe C), and 817 bases from Exon 18 to 20 (Probe D). *DCX* was used as a positive control, and a probe was

generated by amplifying 550 bases of Exon 7. I used the following primers to amplify cDNA using ExTaq polymerase (Takara):

	Forward	Reverse
Probe A	GCGAGTGAGACACAAGAAAAG	TGACCAGCTTGGGTCGAATG
Probe B	CCGGAGTGAGGAGTGAGTGTG	CTTCTATGAGCTCTAACATGGACAC
Probe C	CCCCTCTCGTCGGATGATTTG	TTCCCTTCCAGACATAGTCAC
Probe D	CTCCCAGAAAATGAGCATCAG	GATGGGTGCATCTGCTGATGC
Probe DCX	TACCTGCCGCTGTCATTGGAT	CAATACACTGGGGGCTCAATT

Cycling conditions:

1. 98°C, 10 seconds
2. 50°C, 30 seconds
3. 72°C, 30 seconds

Repeat steps 2 and 4 35 times.

The fragments were subsequently purified with the Wizard Gel and PCR purification Kit (Promega), cloned into TArget Clone plasmid (Toyobo), and grown overnight on LB plates with ampicillin and X-gal/IPTG complex. Following miniprep, the samples were reverse-transcripted using T3 or T7 RNA polymerase (Roche). Plasmids *in vitro* transcripted with T3 RNA polymerase were linearized with *EcoRV* (NEB) whereas samples transcripted with T7 RNA polymerase were linearized with *NotI* (NEB).

In situ hybridization

I performed *in situ* hybridization according to established protocols (Matsuo, 2015). Briefly, C57BL/6J mice were sacrificed at E14.5, P0, P7, P14, and P30, their brain paraffinized overnight using SAKURA Tissue-Tek VIP 5 (Sakura Finetec), mounted into paraffin blocks with the Thermo Scientific™ HistoStar™, and cut in 8 um sections mounted on glass with Auto Slide Preparation System AS-410 (Dainippoin Seiki). The hybridization and staining stages were performed with DISCOVERY ULTRA Ventana (Roche) according to the manufacturer's specifications. In brief, the DIG-labelled probes were then hybridized for 12 hours using the RiboMap Kit (Roche) at 70°C with a probe concentration of 100 ng/ml. Then, the slides were incubated with anti-DIG antibody (Roche, 1:2000) at 37°C for 2 hours and counterstained with RiboBlue Kit (Roche). Coverslips were manually applied, and detection was performed using Keyence BZ-X800 All-in-one microscope at 10x magnification in bright field.

In utero electroporation

In utero electroporation was performed as previously described (Tabata and Nakajima, 2001; Tabata and Nakajima, 2003), Pregnant ICR mice (Japan SCL) were deeply anesthetized with Isoflurane to inject each embryo with 1 ug of plasmids (pCAG-DCLK1-L-Myc-T2A-EGFP, pCAG-DCL-Myc-T2A-EGFP, pCAG-CPG16-Myc-T2A-EGFP, pCAG-CARP-Myc-T2A-EGFP, pCAG-DCLK1-L-D511A-Myc-T2A-EGFP), mixed with PBS and Fast Green (10% final concentration) for a total of 40 ul. E13.5 pups were

electroporated in the Ventricular Zone using NepaGene NEPA21 Type II with the following conditions:

Voltage	Pulse	Pulse interval	Number of pulses	Decay interval
40.0 V	50.0 ms	950.0 ms	5	0%

The animals were then sacrificed at E16.5 and E18.5 and the embryos harvested by Cesarean section, the uterine horn then immersed first in 1xPBS overnight at 4°C, and then in 4% PFA for two days at 4°C.

Immunohistochemistry and statistics

The electroplated animals' brains were dissected, and coronal sections of 100 um were made by vibratome and conserved in PBS with 0.1% Sodium Azide at 4°C. Each section was first permeabilized with 0.1% Triton X-100 in PBS, and then blocked in PBS with 0.3% Triton X-100, 3% Normal Donkey Serum, and 3% BSA. Immunohistochemical stains were performed with the following primary antibodies:

Chicken anti-GFP antibody (Abcam, 1:2000)

Rabbit anti-DCLK1 (C-term; Abcam, 1:2000)

Mouse anti-Myc-tag 9E10 (Jackson Laboratories, 1:250)

Rabbit anti-PAX6 (Covance, 1:500)

Mouse anti-MAP2 2a+2b (Sigma-Aldrich, 1:500)

Incubation lasted for 3 days at 4°C with gentle agitation. Subsequently, the following secondary antibodies were used:

Alexa Fluor 488 anti-chicken IgY (Jackson, 1:2000)

Alexa 555 anti-mouse IgG (invitrogen, 1:500)

Alexa 633 anti-rat IgG (Invitrogen, 1:2000)

Alexa 647 anti-rabbit IgG (Invitrogen, 1:500)

DAPI (Thermo Fisher, 1:2000).

For all statistical analysis, for each sample, 8 pups from 3 or more independent experiments were used. Coronal sections 100 um in thickness were acquired and imaged by confocal microscopy on a Leica SP8 confocal microscope, and a column 200 um in width was extracted. Cells were then counted using the Cell Counter plugin in FIJI and divided in three regions: VZ/SVZ, IZ, and SP/CP, the percentage of cells in each region being determined as the number of electroporated cells in each region divided by the total number of electroporated cells in the whole cortical wall. Using a custom Python script, I assessed the statistical significance by applying one-way Anova, with a test significance of 1%, and plotted the results with error bars indicating the standard error of the mean (SEM). In each plot, the statistical significance is represented by a **, including p value results. My algorithm also created a table for each time point and for each condition containing the total number of neurons in a specific zone for each sample. I then calculated percentage per region, assembled by time point into a single Pandas dataframe with the included metadata of time point and condition. Then, for each set of conditions and for each time point I produced a plot by sorting the dataframe according

to the metadata. This was then arranged into a nested bar plot in which for each condition the mean percentage over sample for this condition over the regions were plotted. In this case, the error bar was given as the standard deviation over samples for each region for each condition.

To quantify the fluorescence intensity of IUE, I used the protocol previously described by Crowe and Yue, 2019. Briefly, anti-Myc and anti-GFP stained confocal images were imported in Fiji, deconvoluted, and a threshold with the minimum value set to 0 and the maximum experimentally determined was applied to eliminate background. Then, the area and mean grey values for anti-Myc and anti-EGFP stains were measured and Myc/GFP was calculated. Statistical significance was calculated by one-way Anova.

Primary culture

I isolated cortical neurons from E15 mouse embryos and cultured them as previously described (Kaiser et al., 2013). The day before culturing I placed glass coverslips measuring 13 mm in diameter in 35 mm dishes and coated them with 1mg/ml poly-D-lysine (Sigma-Aldrich) in Borate Buffer. After 1 hour of incubation at room temperature, I changed the buffer solution to the same Neurobasal (Gibco) used for culturing. This Neurobasal medium contains penicillin and streptomycin, glutamine, and B27 supplement (Gibco). To generate the culture, C57BL/6J (SLC Japan) mouse embryos of both sexes were removed by Cesarean section and decapitated. The cortex was manually dissected under a microscope and placed in HBSS (Invitrogen) on ice. After decanting briefly on ice, the samples were incubated in a previously equilibrated

Papain solution (20 U, Worthington) in Earle's Balanced Salt Solution (EBSS; Gibco) with bicarbonate and phenol red (600ul/embryo), with 0.1% 500mM EDTA pH 7.0, and L-Cysteine at 37°C for 15 minutes. In the meantime, two solutions were prepared: 10/10 solution containing EBSS, 10 ug/ml Trypsin inhibitor (Invitrogen) and 0.1% BSA (Invitrogen), and a 1/1 solution, composed of 90% EBSS, 1% 10/10 solution, and DNase. Then, the supernatant was removed, resuspended in 1/1 solution, and triturated with a fire polished glass pipette tip. Prior to plating, cells underwent Nucleofection™ with P3 Primary Cell 4D-Nucleofector X Kit (Lonza). 1 ug of each plasmid (described above) was transfected to 2.5x10^5 cells using 4D-Nucleofector X Unit (Lonza). All cells were finally plated on 35 mm petri plates previously prepared. Cultures were maintained in Neurobasal medium containing Penicillin, Streptomycin, Glutamine, and B27 supplement (all from Gibco) and grown until DIV7 at 37°C with 5% CO2.

Immunocytochemistry

Neurons were fixed at DIV7 with 4% PFA in PBS, rinsed in PBS, blocked with 1% bovine serum albumin, 0.1% Triton X-100 in PBS, and stained with Chicken anti-GFP antibody (Abcam, 1:2000) and Mouse anti-Myc-tag 9E10 (Jackson Laboratories, 1:250). After secondary antibody incubation, images were acquired with Leica SP8 confocal microscope and processed with FIJI.

Sholl analysis and statistics

Images were obtained using a Leica SP8 confocal microscope. Confocal images of labelled cells were imported into Fiji, deconvoluted as described in Dougherty, 2005, and traced using the Simple Neurite Tracer ver.3.1.3 (Longair et al., 2011). To do so, z-stacks were transformed into 3D images which I manually traced and reconstructed by tracing all processes starting from the soma. The soma center was manually defined as an extension of the longest primary projection, as described (Binley et al., 2014), and excluded from the Sholl analysis computation, but used as the center for the analysis, which was performed with the Sholl plug-in from FIJI release 3.6.12 (Ferreira et al., 2014). The analysis is performed by applying concentric rings spaced 10 um from one another and counting the number of processes that intersect each ring. Subsequently, a linear Sholl plot was created by fitting the data to a polynomial function as previously described (Ristanović et al., 2006). In addition, total projection length was calculated using the Single Neurite Tracer path tool and plotted to compare neurite length across the different constructs.

To asset the statistical power of the Sholl analysis, a table was created for each test condition containing the total length of each sample. Each of the tables were then gathered into a Pandas dataframe with a “type” column metadata used to sort the data. I then sorted the data frame according to condition and produced a mean over samples for each condition. Then, the means over sample per condition were plotted with error bar (standard deviation over samples). The statistical significance was then tested using ANOVA (constructs vs. control) with a p value threshold of 1%.

RESULTS

In silico analysis reveals unique expression dynamics of DCLK isoforms in developing mouse cortex

Previous works assert that the murine *Dclk1* gene consists of 20 exons that undergo alternative splicing, resulting in multiple different isoforms (Burgess and Reiner, 2002). According to the latest data in NCBI RefSeq updated in November 2020, at least 12 different isoforms are potentially derived from these exons (Table 1). These isoforms can be separated into 4 groups according to their domains (Fig. 1), namely DCLK1-L (Variant 1), DCL (Variant 4), CPG16 (Variant 13), and CARP (Variant 7). Previous studies also suggest that the transcripts of the *Dclk1* gene are differentially spliced in the developmental stages and tissues, with the long isoform DCLK1-L and DCL being predominantly expressed embryonically, and CPG16 being considered the adult form (Burgess and Reiner, 2002; Engels et al., 2004). To examine the quantitative expression levels of the isoforms in a temporal manner, I took advantage of publicly available RNA sequencing (RNA-Seq) data, assessing the data bioinformatically. In order to do so, I re-analyzed the transcriptome data of the mouse cerebral cortex in five developmental stages, at E14.5, P0, P7, P15, and P30, pulled from SRA (Yan et al., 2015). The quantification of the expression of splicing variants requires a special computation when RNA-Seq data are generated by short-read sequencers because the majority of the reads are mapped on the exons contributing to multiple variants and the variant-specific

expression is measured by the minor reads mapped on the unique exons specific to a given variant and on the exon junctions characterizing alternative splicing.

To extract this information from transcriptome data and plot it into one readable form, I took advantage of the Sashimi plot, which was originally developed as a part of the MISO framework (Katz et al., 2010). The Sashimi plot provides two major types of information. First, the histogram represents the abundance of the reads mapped on exons. Second, arches connecting exons represent the number of reads mapped precisely on a junction between given exons (Fig. 4B). In order to gather additional information to compare the abundance of different variants, I first identified the critical regions relevant to this analysis in exons 5 to 9, which are located in the middle of the regions encoding for major MT-binding and kinase domains. The first two isoform groups, DCLK1-L and DCL, share exon 1 to 5 followed by 7, whereas the second group, with CPG16 and CARP, start their transcription from exon 6 followed by 7. Therefore, the read depth on the junctions between exon 5 and 7 (Fig. 4A magenta) and between exon 6 and 7 (Fig. 4A blue) are important to calculate the abundance of the different groups. The termination site of transcripts is also fundamental in discriminating isoform groups: DCL and CARP terminate their transcription in exon 8, but the exon is skipped in the other two DCLK1-L and CPG16, making the junctions of exon 7 and 8 (Fig. 4A green) and of exon 7 and 9 (Fig. 4A yellow) the unique identifiers.

To further study the expression dynamics of the isoforms, I also normalized the read number on the identifier exon junctions as a percentage of the total reads in a given sample (Fig. 4C). This clearly indicates that the abundance of DCLK1-L and CPG16

isoforms is much greater than that of DCL and CARP. In particular, CARP appears to be the most minor isoform, its abundance negligible in relationship to the other ones. In addition, it is probable that the read numbers on the junctions of exon 7 and 8 (DCL and CARP) and that of exon 6 and 7 reflected (CPG16 and CARP) mirror the relatively stable expression of DCL and the rapid upregulation of CPG16 during the first postnatal two weeks, respectively. To sum up, DCLK1-L shows a stable and high level of expression in the prenatal development, making it the major isoform at that stage, and CPG16 becomes the most abundant one in the postnatal maturation. It is plausible to also conclude that DCL and CARP provide minor contributions relative to the other two at the time points examined. In addition, this data strongly suggests that the transcriptome analysis using the exon junctions unique for each isoform can be applied for quantitative analysis of DCLK1 isoforms.

To complement the findings put forth by the *in silico* analysis, I also sought to directly test the abundance of the isoforms by Western blot (WB) using two antibodies specifically recognizing the N-terminus and C-terminus of DCLK1-L (Fig. 5A,B). The samples were harvested from whole cortexes at the same stages used in the transcriptome study, and two distinct antibodies are used, to detect 3 out of 4 variants. The N-term antibody shows two bands: one with slightly upregulated level of signal at approximately 85 kDa, consistent to the maintained expression of DCLK1-L throughout the embryonic to postnatal stages, and a faint but detectable signal embryonically and at P0, at 40 kDa, which is the expected size of DCL. The second antibody binds on the C-term, and therefore has affinity for both DCLK1-L and CPG16. With this antibody it is possible to see the same 85 kDa band as before (DCLK1-L), in addition to a second band

at 50 kDa. This second band shows an increase over time, possibly reflecting the strong upregulation of CPG16 in the postnatal stages. With these antibodies it is not possible to examine CARP, because of the lack of epitope for either antibody. This WB was also normalized against actin control and the normalized intensity of the immunoblot bands was quantified (Fig. 5C, D). In summary, the protein analysis confirms the trend found in the isoform-specific transcriptome, and is consistent with previous reports (Shin et al., 2013; Koizumi et al., 2017), according to which the DCLK1-L expression level is gradually upregulated in the early postnatal stages, whereas DCL expression is immediately down-regulated in the late embryonic stage. On the other hand, CPG16 level is up-regulated postnatally. It is interesting to note that although DCL protein levels were quickly down-regulated in the early postnatal stage, transcriptomic analysis revealed substantial expression of DCL postnatally (Fig. 4B). This somewhat contradictory finding poses the question of whether DCL protein levels might be influenced by post-transcriptional controls such as degradation of mRNAs or proteins postnatally.

Dclk1 isoforms are regionally segregated in the cerebral cortex and the hippocampus

The detailed transcriptome analysis revealed variant-specific temporal dynamics during the cortical development, however, the data is derived from bulk samples of cortical tissue containing many different cell types. To have a more precise idea of the expression in different cell types, I sought to study the spatial distribution of *Dclk1*

isoforms by *in situ* hybridization (ISH) using specific probes for the different *Dclk1* isoforms.

The shared usage of exons among the *Dclk1* variants made designing specific probes for each variant impossible. To minimize confounding effects, I generated four different probes, which reasonably discriminate for four major isoforms (Table 2). Probe A is designed to recognize exons 1 to 3 and hence DCLK1-L and DCL, which share these exons, are detected. Similarly, probe B, C, and D are designed to recognize exon 6, 8, and 18-to-20 (Fig. 6).

First, I examined the cortex. Probe A, which recognizes DCLK1-L and DCL, shows a prominent signal in P7 cortex compared to P30 (Fig. 7), whereas Probe B, which is designed to recognize CPG16 and CARP, shows signals in P30. In addition, at P7 the signal is below detectability (Fig. 7). No detectable sense probe signals were detected for any of the four Probes in P7 brain, indicating that the signals observed in the brain are specific for to the Probes and not backgroud (Fig. 10). By comparing the blotting data and the transcriptome data with ISH results, I am able to infer that Probe A's signal in P7 cortex is most likely due to DCLK1-L expression, as both blotting and transcriptome data indicate that DCLK1-L expression is much higher than DCL at that time point. Similarly, since the CPG16 expression level is much higher than that of CARP at P7 and P30 in the cortex, Probe B signal at P30 is likely to represent CPG16 expression. Of note, Probe A's signal can be predominantly observed in the upper layers of the cortex at P7, whereas Probe B's signal is more evenly distributed in P30 cortex

(Fig. 7). This likely means that DCLK1-L and CPG16 may exert their functions not only in different time points but also in different neuronal populations.

Next, I also examined the signal in the whole brain at 5 different development stages (Fig. 8). I was able to detect marked spatial segregation with the different probes: for instance, Probe A and D show comparable signal between the olfactory bulb and the cortex at P7. On the other hand, Probe B shows prominent signal in the cerebellum at P15-30, with dominant signal in the Purkinje cells layer (Fig. 8A). This is in contrast to Probe C, which shows signal predominantly in the granule cell layer. The hippocampus shows particularly interesting spatial segregation of the signal (Fig. 9). Probe A and Probe D show an ubiquitous signal in all regions of the hippocampus, whereas Probe B and Probe C signals were exclusively segregated in the hippocampal regions: Probe B was observed in the CA1-3, and Probe C signal was mainly localized in the dentate gyrus (DG) and CA1. Because Probe B detects CPG16 and CARP, whereas Probe C detects DCL and CARP (Fig. 6), it is likely that Probe B signal and Probe C signal in the hippocampus represent CPG16 and DCL, respectively (Table 3).

Overexpression of DCLK1-L alters neural migration in a kinase activity-dependent manner

The findings presented in the previous section indicate that the splicing variants of the *Dclk1* gene are dynamically regulated during cortical development, which suggests that alternative splicing of *Dclk1* produces a variety of proteins containing

different combinations of functional domains, and these potentially contribute to multiple aspects of brain development. In order to clarify the *in vivo* functions of the different splice variants, each variant C-terminally tagged with Myc together with EGFP was electroporated into the embryonic cortexes at E13.5 (Fig. 11A). Subsequently, I observed the distribution and the morphology of EGFP-labeled neurons generated by the electroporated cortical progenitors at E18.5 (Fig. 11C). I then quantified the number of neurons in different regions of the cortex, namely the ventricular and sub-ventricular zone (VZ/SVZ), the intermediate zone (IZ), and the region from the sub-plate and the pial end of the cortical plate (SP/CP). First, I noticed a clear alteration in the neuronal distribution in the over-expression of DCLK1-L, in comparison to the control. Quantitative analysis revealed that DCLK1-L induces an ectopic accumulation of neurons immediately under the sub-plate, suggesting that this variant perturbs the entry of neurons into the SP from the IZ (Fig. 11D). Concomitantly, the neurons showing stalled migration in the IZ demonstrate a multipolar morphology (Fig. 11C inset), also indicating a failure in the transition from multipolar to bipolar which is necessary for entry into the SP (Cooper, 2014). I decided to investigate this phenomenon further and also address whether the kinase activity was necessary to give rise to this phenotype. To do so, I generated a Kinase-dead version of DCLK1-L. In this case, the crucial residue (position 511 for DCLK1-L) in the kinase domain was replaced from aspartate to alanine. Interestingly, this phenotype caused by DCLK1-L over-expression is diminished when the kinase activity is impaired by the amino acid substitution: the kinase-dead mutant shows no overt changes in the neuronal distribution compared to the control, and thus I concluded that the migration defect in the over-expression of DCLK1-L requires its

kinase activity. Second, DCL, which has the MT-binding domain but lacks the kinase domain, demonstrates a similar but less evident trend of migration failure as in the over-expression of DCLK1-L (Fig. 11E-F). No striking difference was found in the over-expression of CPG16 in terms of the neuronal distribution (Fig. 11G-H). Lastly, the over-expression of the shortest CARP, which contains neither the MT-binding nor kinase domains, does not show any defects in migration and morphology (Fig. 11I-J). In summary, among the four splice variants examined in this study, only DCLK1-L demonstrates the potential to alter the pattern of radial migration and in a kinase-dependent manner. Since CPG16, which possesses a kinase domain but lacks the MT-binding domain, does not show any phenotypic impact, I concluded that DCLK1-L regulates cortical radial migration through a combinatorial function of MT-binding and kinase domains.

To confirm that the observed phenotypes were not due to a difference in the expression level of the proteins, I quantified the level of fluorescence of the anti-GFP and anti-Myc tag stain and compared it across the different samples using a semi-quantitative approach of Myc signal divided by GFP signal and arbitrary units (Cregger et al., 2006; Taylor and Levenson 2006; Braun et al., 2013; Bauman et al., 2016; Pike et al., 2017). Similar levels of protein expression were found, confirming the reliability of my data, as the phenotypic difference therefore reflects the functional difference of each isoform *in vivo* (Fig. 12).

Overexpression of DCLK1-L in cultured cortical neurons causes an increment of dendrite branching in a kinase activity-dependent manner

The *in vivo* overexpression study indicated that the long DCLK1-L functionally contributes to cortical development in a splicing-specific manner through its kinase activity. Next, I examined the functional involvement of *Dclk1* splice variants at the single neuron level. I isolated cortical neurons from E15 mouse cerebral cortex and cultured them *in vitro* with overexpression of the same four *Dclk1* variants as in the *in vivo* study. The expression constructs were introduced to the dissociated cortical neurons by electroporation immediately before seeding in the culture dish (Fig. 13A). The total neurite length and branching were then quantified on the seventh day of the culture (Fig. 13B). I observed a similar degree of the phenotypic impact on the cultured neurons as in the *in vivo* study (Fig. 13C-F). The neurite length is significantly increased by the introduction of DCLK1-L and this effect relies on its kinase activity (Fig. 13B). Additionally, the neurite complexity is increased by massive arborization in the over-expression of DCLK1-L (Fig. 13C), and again this phenotype is completely diminished in the kinase-dead mutant. Therefore, DCLK1-L not only elongates the neurite but also increases the arborization through its kinase activity.

The over-expression of DCL, which encodes only the MT-binding domain, also increased the dendritic branching but the effect is more concentrated on the proximal region close to the cell body compared to the case of DCLK1-L (Fig. 13D). Intriguingly,

DCL shows an impact only on the neurite complexity but not on the total length. The kinase domain-containing CPG16 demonstrates both elongation and enhancement of the complexity of dendritic arbors as well (Fig. 13E), but nevertheless the neurite branching is less prominent in the distal region compared to DCLK1-L. Lastly, CARP does not show any changes from the control as observed for *in vivo* over-expression (Fig. 13F). Finally, quantitative data of Myc-tagged isoforms against beta actin on the blots indicated no significant difference in expression levels of each isoform in cultured neurons, suggesting that the phenotypic differences observed comes from functional differences of each isoform, rather than differences in expression levels (Fig. 14).

Taken all together, DCLK1-L shows the most eminent impact both on the neurite length and complexity, among the four variants tested. Though their impacts are relatively weaker than that of DCLK1-L, the effects caused by DCL, which contains only the MT-binding domain, and CPG16, which possesses only the kinase domain, are not negligible. This could mean that the MT-binding domain alone is sufficient to induce a proximal neurite branching and the kinase domain alone can elongate and increase the number of processes in a neurite, and so this data suggest that the two domains act synergistically in the over-expression of DCLK1-L.

DISCUSSION

In this study, I utilized multiple different methods to dissect the expression and function of the DCLK1 isoforms *in vivo*. I report the expression dynamics of the four major *Dclk1* variants across several time points in the developing murine brain, and investigate the functional roles exerted by the different variants. My results show that the variants have segregated expressions, both temporally and spatially, although additional functional studies are required to completely understand the role of elusive isoforms such as CPG16 and CARP. In particular, my *in silico* analysis successfully highlighted exon-exon junctions which can be used to selectively extract each variant's expression dynamics. To my knowledge, this is a novel approach for splice isoform analysis which can be easily implemented and poses several advantages. First, using informatics for transcriptome analysis provided us with a powerful and unbiased way to study the expression patterns of the different splicing variants. Thanks to recent advancements, it is now possible to perform systematic studies at different time points targeting several loci at once, with the added ability to precisely quantify expression of different exon as well as exon-exon junctions. Second, the use of the Sashimi plot is an easy and reliable way to assess the precise expression pattern of alternative splicing at the mRNA level, with great potential for parallelization and the ability to uncover new variants. Downstream methods such as WB can also be used to determine protein expression levels though they rely heavily on the quality and specificity of the antibody, not to mention that discrepancies between the transcriptome and the proteome can arise. In

clinical practice, transcriptome analysis is also becoming more widespread especially in cancer and complex diseases diagnosis (Chhatriya et al, 2020; Rathi et al. 2020).

This data is further reinforced and enriched by both WB and ISH. Looking at the cortex, on one hand, my ISH results suggest DCLK1-L expression is localized in the relatively upper layers in P7 cortex (layers II/III to V), and gradually wanes by P30. On the other hand, CPG16 is strongly upregulated from P7, and its localization appears to be more evenly distributed in the cortex. These diametrically opposite patterns seem to point to the directions of functionally different roles exerted by these two isoforms, both in the development and in the mature brain. In fact, a plethora of studies highlight the role of DCLK1-L in synapse maturation, neurite growth, and neurogenesis by regulating mitotic spindles (Shin et al., 2013; Koizumi et al., 2017; Shu et al., 2006). Therefore, it is possible plausible that DCLK1-L expression declines in the mature neurons to maintain functional circuits, as opposed to CPG16. The latter's *in vivo* function in brain development remains elusive, with its kinase target still unknown, but the expression pattern of CPG16 seems to imply that it is required for the maturation as well as the formation of new synapses. In fact, the first two postnatal weeks are marked by active remodeling in the mouse brain, and especially in pyramidal neurons (Kroon et al., 2019), though CPG16's role in these functions is to date merely speculative.

Another interesting result of this study is the peculiar spatial segregation of signal in the hippocampus. At P30, CPG16 is largely expressed in the CA1-3 regions, but absent from the DG, whereas DCLK1-L is expressed in all fields of the hippocampus. DCL, on the other hand, is predominantly in the CA1 and DG, which is consistent with previous reports indicating that DCL is expressed in the neurogenic regions including

the DG in the adult brain and that it functions in adult hippocampus neurogenesis (Saaltink et al., 2012; Saaltink et al., 2020). This is particularly relevant because of the implication of the hippocampus in several NDDs (Li et al., 2019). Several SNPs conserved across patients with bipolar disorder and schizophrenia are strongly associated with intron 3, and these two pathologies in turn are known for their alteration of the normal development of the DG. The DG is also a crucial area in cognition (Danielson et al, 2016). In contrast, CPG16's localization in the CA field seems to implicate that CPG16 is involved in plasticity, since this isoform is upregulated by stimuli inducing LTP (Hevroni et al., 1998) and the CA1-3 region is a center for learning and memory, particularly in learning and memory mediated by CA1-3 pyramidal neurons (Soltesz and Losonczy, 2018). The absence of CPG16 from the important adult staminal niche, the DG, also points in the direction of its roles being more related to plasticity and synapse formation than migration and maturation, as it has been postulated previously (Silverman et al., 1999). CARP, on the other hand, was not detected in my analysis, and *in silico* data suggests very low expression. Over the years, several reports have shown that CARP is associated with apoptotic cells (Schenk et al., 2007), is upregulated by kainite-induced seizures, and helps memory consolidation, findings which suggest a role in neuronal plasticity (Vreugdenhil et al., 1999; Schenk et al., 2011). While adult, stimulus-dependent expression has been reported (Schenk et al., 2010), endogenous, *in vivo* expression of this isoform has not been reported yet, but its Ser/Pro rich structures seem to indicate its role in protein-protein interactions, and therefore it is plausible that its expression may only be detectable under specific circumstances and as a result of specific stimuli.

Additionally, over-expression of DCLK1-L, but not DCL, CPG16, or CARP, in progenitors caused severe migration defects. A previous study showed that DCLK1-L-EGFP over-expression in the cortical progenitor cells induces the differentiation of cortical progenitors, altering the rate of asymmetric division and accelerating cell migration (Shu et al. 2006). This results could potentially explain the similar number of cells observed in the CP/SP in control and DCLK1-L gain-of-function. While this is a compelling argument which would complement the phenotype observed in the DCLK1-L overexpression, the current results neither corroborate nor dispute it. On the other hand, other previous studies have suggested that migrating cortical neurons typically transform from multipolar to bipolar morphology in the SVZ and IZ, a transition which might promote the entry into the CP (Nadarajah et al., 2001; Noctor et al., 2004). Given that I have observed neurons with multipolar morphology mainly in the IZ in DCLK1-L overexpression, another potential scenario is that DCLK1-L overexpression might perturb the multipolar-to-bipolar shape transition. In addition, my *in vitro* experiment suggests that DCLK1- L overexpression enhances dendrite growth and branching in cultured cortical neurons , which is consistent with this observation.

While the precise mechanism underlying how DCLK1-L overexpression causes this phenotype remains to be understood, my results suggest that such migration appears to occur in a kinase-dependent fashion, as no obvious defects in neither cortical neuron migration nor in branching phenotypes in cultured neurons were observed by over-expressing the kinase-dead version of DCLK1-L. It is thus more likely that DCLK1-L over-expression affects neuronal migration and dendrite branching via its kinase activity, both

dependently and independently of its catalytic activity. This area is still very debated: previously it has been shown that DCLK1-L promotes dendritic growth and branching via Kinesin-3-mediated vesicle transports in dendrites (Lipka et al., 2016), independently from the kinase activity, so it is reasonable to think that DCLK1-L may promote dendritic growth and branching in both kinase activity-dependent and -independent ways. There is, in fact, evidence for both pathways: previously, MAP7D1 has been identified as a substrate of DCLK1-L in mouse brain using co-immunoprecipitation and subsequent mass-spectrometry, together with *in vivo* and *in vitro* evidence that this phosphorylation promotes axon elongation in developing cortical neurons (Koizumi et al., 2017). However, the role of the DCLK1-L-mediated MAP7D1 phosphorylation in radial migration has yet to be examined *in vivo* (Koizumi et al., 2017). Therefore, a compelling field of research would be examining whether DCLK1-L does in fact perturb radial migration by phosphorylating MAP7D1 or other potential candidates. On the other hand, non-catalytic kinase activity is also likely to play an important role, and interactions between the kinase domain and α-SYN have been recently discovered (Vázquez-Vélez et al., 2020). This last discovery is particularly fascinating, as it appears that the kinase domain can regulate α-SYN independently of both its own catalytic activity and the MT-domain.

Another interesting aspect worth investigating is how DCLK1-L regulates neuronal migration. It is possible to speculate that DCLK1-L may regulate MT bundling through either autophosphorylation or by its phosphorylation of DCX (Koizumi et al., 2017), which is also confirmed by the lack of migration defect in DCLK1-L kinase dead and CPG16 overexpression. Together, this data suggests that a cooperation between the two

domains has to take place to exert DCLK1-L roles. In addition, a recent study (Patel et al., 2016) confirmed the high degree of cooperativity between the two domains, with the kinase domain probably acting with an autoinhibitory role on the MT-domain affinity for tubulin.

In addition, this study also contributes to the understanding of the role of *DCLK1* in the pathophysiology of a variety of neurodevelopmental disorders such as schizophrenia, ADHD, and bipolar disorder, given the multiple SNPs on this gene which are associated with these pathologies (Håvik et al., 2012). Several markers on the *DCLK1* gene show a strong association with higher cognitive functions as well as memory (Le Hellard et al., 2009). Another compelling argument for further characterizing the expression dynamics of the different isoforms is brought forth by a previous transcriptome study in schizophrenia (Wu et al., 2012), which highlighted the alternative promoter usage and the upregulation of certain isoforms, DCLK1-L in particular, in schizophrenia patients. Thus, uncovering the functional differences between the isoforms is important to understand their roles in development and in pathology, especially has it has become more and more clear that genetic susceptibility is a key factor in the etiology of NDDs.

CONCLUSIONS

In summary, in this study I dissected the expression pattern of the four major *Dclk1* variants in the development of the mouse brain by a variety of methods. Using available data which I newly analyzed *in silico*, in combination with my own data from *in vitro*, *in vivo*, and biochemical techniques, I was able to show how the expression of the isoforms segregate both temporally and spatially. This in turn points to the possible function of each variant, and I provided evidence that overexpression of DCLK1-L in the developing cortex impairs the correct radial migration of developing cortical neurons in a kinase-dependent manner. As the function of other isoform remains elusive, this study also shows how harnessing the power of publicly available deep sequencing and RNAseq data platforms can further studies aiming to elucidate both isoform-specific expression and function in the developing brain.

ACKNOWLEDGEMENTS

First and foremost, I would like to thank Dr. Emoto for fostering my interest in Neuroscience and research in general, making it possible for me to pursue this academic milestone in his lab. I would also like to thank former members of the lab, in particular Dr. Koizumi, who supervised me in my first year of PhD and provided the DCLK1 KO mice, not to mention fundamental insight in the making of this dissertation, and Dr. Togashi, for his instrumental help in making the electroporation constructs.

I am also particularly grateful to Dr. Suzuki, for critically reading this dissertation, as well as providing insight for *in vivo* manipulations and IUE.

I am truly grateful to the rest of Emoto lab (the laboratory of Brain function, Department of Biological Sciences, Graduate School of Science, The University of Tokyo), for their jovial support as well as critical feedback to my research.

Finally, I'd like to thank my husband Carl for buying me plenty of satsuma imo to sustain me during this doctorate.

FIGURES

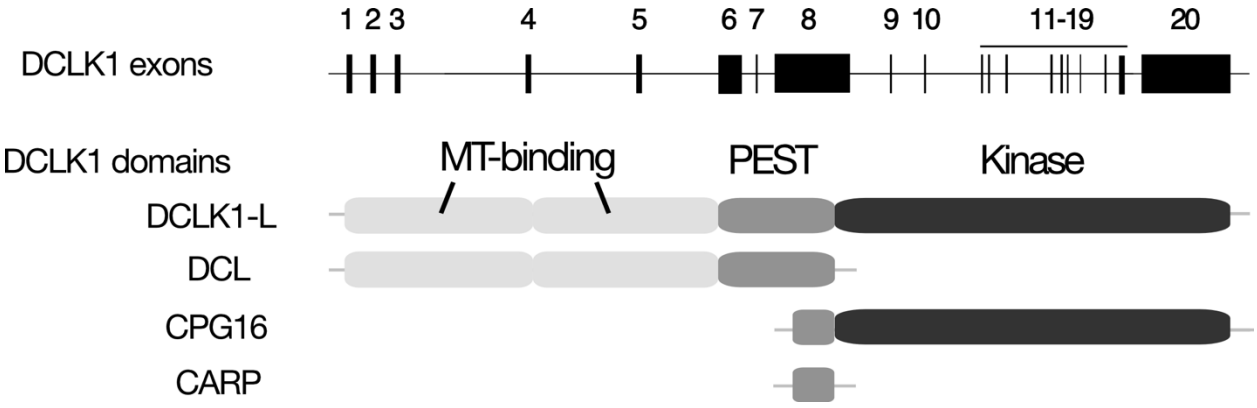

Figure 1. Schematic representation of the exon usage of the predominant DCLK1 variants and their domain structure.

In this study, I focus on the four major variants of the *Dclk1* gene: DCLK1-L, DCL, CPG16, and CARP. These 4 variants are varied in their structure and exon usage: a long isoform called DCLK1-L (MT domain, S/T domain, Kinase domain); the short CPG16 (S/T domain and Kinase; DCL (MT domain only), and CARP (short S/T domain and part of the kinase domain).

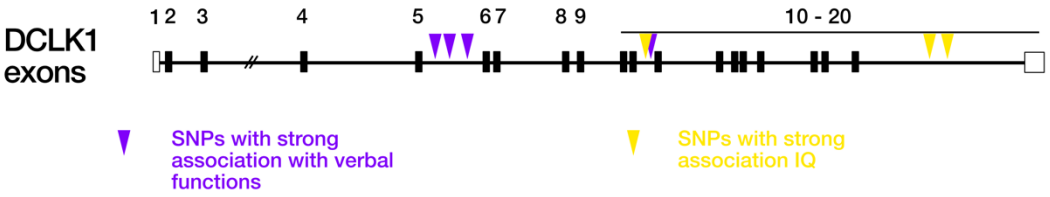

Figure 2. SNPs on *DCLK1* are related to higher function.

Several SNPs have been reported in literature on the *DCLK1* gene, chiefly related to cognitive functions such as memory and verbal functions.

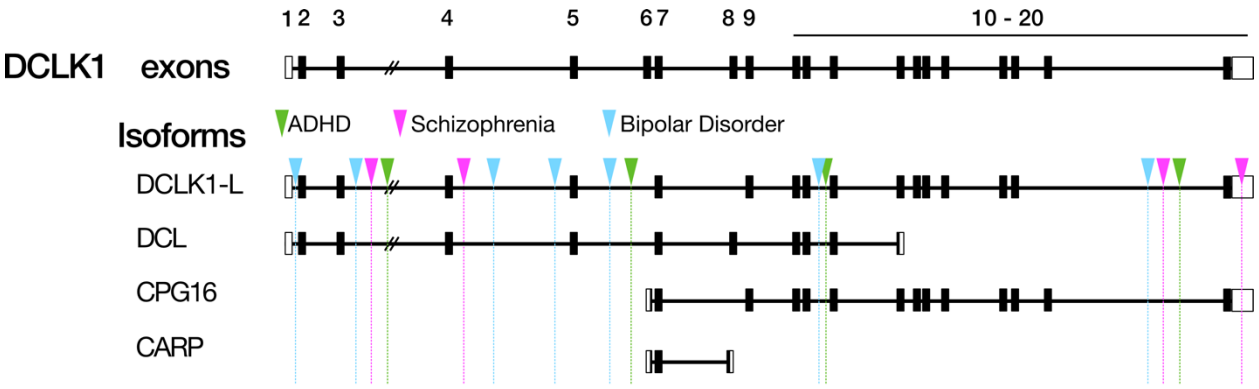

Figure 3. SNPs associated with Neurodevelopmental Disorders on *DCLK1* are conserved across different cohorts of patients.

More recently, GWAS have shed a light on more SNPs conserved in two Scottish cohorts and one Norwegian cohort (Håvik et al., 2012). This data reinforces the preexisting notion that *DCLK1* is involved in the neurodevelopment and in disease, possibly acting on synaptic plasticity.

Table 1

Nomenclature	RefSeq nomenclature	RefGene ID	Exon usage	Domain composition	Signature junctions
DCLK1-L	Variant 1	NM_019978	1-5, 7-18, 20	MT domain, S/T domain, Kinase domain	5-7-9; 18-20
CPG16	Variant 2	NM_001111051	6-18, 20	S/T domain, Kinase domain	6-7; 18-19-20
CPG16	Variant 3	NM_001111052	6-20	S/T domain, Kinase domain	6-7; 18-20
DCL	Variant 4	NM_001111053	1-5, 7-8	MT domain, S/T domain,	5-7-8
DCLK1-L	Variant 5	NM_001195538	1-5, 7-18, 20	MT domain, S/T domain, Kinase domain	5-7; 18-20
CPG16	Variant 6	NM_001195539	6-18, 20	S/T domain, Kinase domain	5-7; 18-20
CARP	Variant 7	NM_001195540	6-8	S/T domain	6-7-8
DCLK1-L	Variant 9	NM_001357466	1-5, 7-20	MT domain, S/T domain, Kinase domain	5-7; 18-19-20
CPG16	Variant 10	NM_001357468	6-20	S/T domain, Kinase domain	6-7-9; 18-20
DCLK1-L	Variant 11	NM_001357469	1-5, 7-20	MT domain, S/T domain, Kinase domain	5-7; 18-19-20
DCLK1-L	Variant 12	NM_001357475	1-5, 7-18, 20	MT domain, S/T domain, Kinase domain	5-7; 18-20
CPG16	Variant 13	NM_001357476	6-20	S/T domain, Kinase domain	6-7; 18-19-10

Table 1. Summary of the different DCLK1 Variants and their exon usage.

Variants can be grouped in 4 groups according to domains: the long isoform group of DCLK1-L (MT domain, S/T domain, Kinase domain) such as Variants 1, 5, 11, and 12; a short group of CPG16 (S/T domain and Kinase) such Variants 2, 3, 6, and 13; DCL (Variant 4; MT domain only) and CARP (Variant 7; short S/T domain and part of the kinase domain).

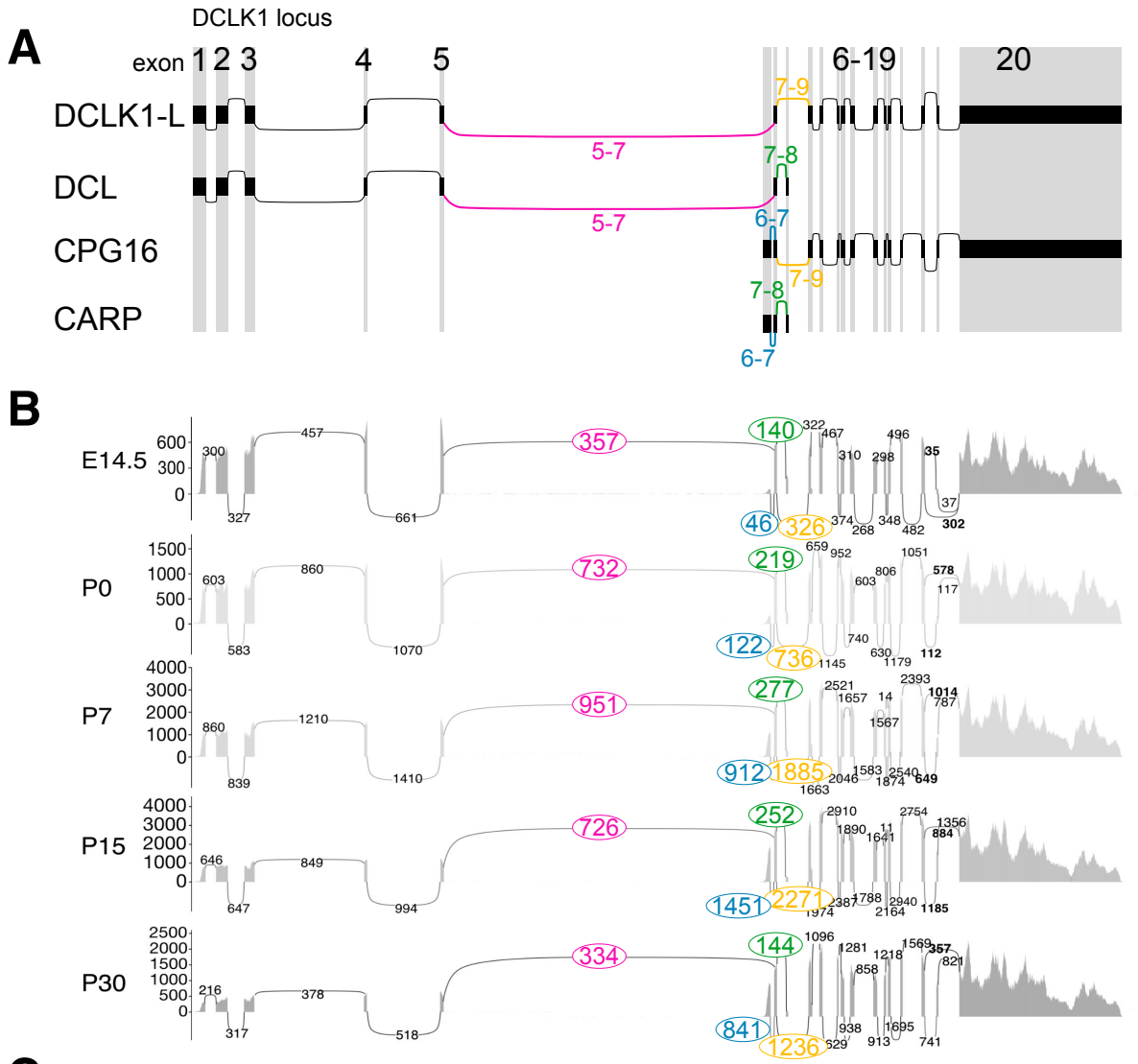
A
DCLK1 locus
exon 1 2 3 4 5 6-19 20
DCLK1-L
DCL
CPG16
CARP
5-7
7-9
7-8
6-7
B
E14.5
P0
P7
P15
P30
C
Relative Reads [Nreads/Ntotal]
E14.5 P0 P7 P14 P30
5-7 (DCLK1-L+DCL)
7-9 (DCLK1-L+CPG16)
7-8 (DCL+CARP)
6-7 (CPG16+CARP)

Figure 4. RNA-Seq data analysis of the expression pattern of the *Dclk1* transcripts in the cortex.

RNA-Seq data is fed into a series of algorithms together with RefSeq annotations. Exon-exon junctions also indicate the read number for each boundary level. Every isoform is characterized by a signature series of junctions. (A): 5-7 for DCLK1-L and DCL (magenta), 6-7 for CPG16 and CARP (blue), 7-8 for DCL and CARP (green), and 7-9 for DCLK1-L and CPG16 (yellow). In addition, Sashimi plot results yield histograms where the per-base coverage is plotted on the y axis, and the genomic coordinates are annotated on the x axis, and relative abundance of expression of each exon can therefore be extracted by comparing the histograms (B). Moreover, the read depth of each exon-exon junction is another indication of the abundance of individual isoforms. (C) Extracting information from the signature exon-exon boundaries helps quantify the expression dynamics at a glance. For example, it is easy to see how CPG16 expression increases postnatally (yellow and blue), whereas CARP expression remains very low (green).

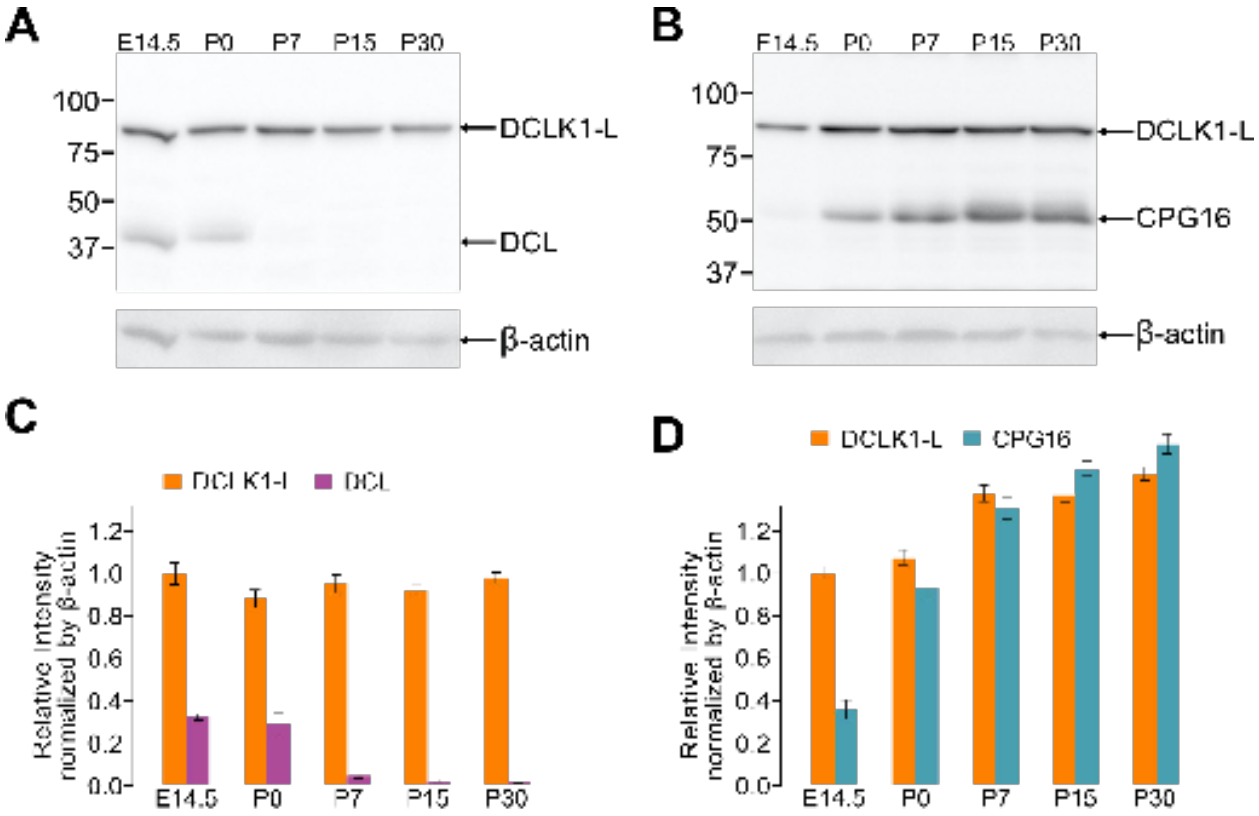

Figure 5. Expression pattern of four DCLK1 isoforms in the cortex.

Two antibodies are used: an N-term antibody, with affinity for DCLK1-L and DCL (A), and a C-term antibody, with affinity for DCLK1-L and CPG16 (B). While DCLK1-L's expression is sustained postnatally, and slightly upregulated, DCL rapidly decreases postnatally. On the other hand, CPG16 increases stably after birth. The quantification graphs (C, D) show the temporal dynamics of the different isoforms against beta-actin, used in this case as loading control (n=3).

	DCLK1-L	DCL	CPG16	CARP	Targeting exons
Probe A	+	+			1,2,3
Probe B			+	+	6
Probe C		+		+	8
Probe D	+		+		18-20

Table 2. Probe design and targeting isoforms.

Because of the identical sequences across different Variants, I designed probes which bind two different Variants and then compared them in pairs to extract information on the spatial pattern of expression. Probe A binds the beginning of the coding region, on exons 1, 2, and 3. On the other hand, Probe B and C bind a single exon, exon 6 and 8 respectively, and therefore have affinity for CPG16 and CARP, and DCL and CARP. Probe D binds DCLK1-L and CPG16, from exon 18 to the 3'UTR.

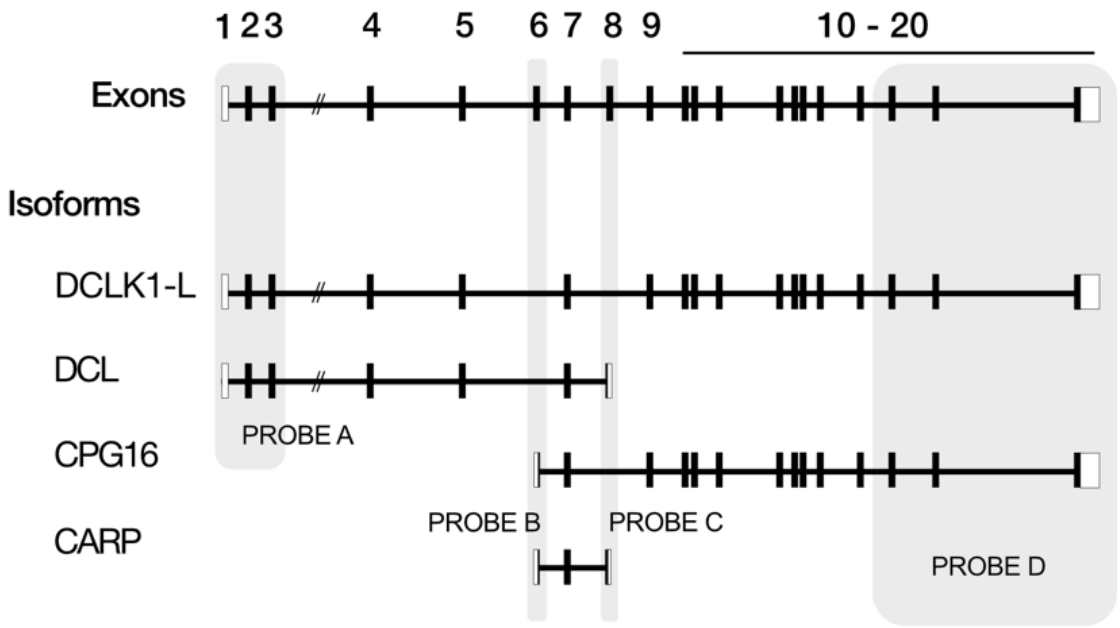

Figure 6. Probe design with targeting exons.

Probe D includes exons 18 and 20 but no exon 19, which makes it specific for the version of DCLK1-L called Variant 1. On the other hand Probe A recognizes DCLK1-L and DCL, Probe B has affinity for CPG16 and CARP, and the latter, together with DCL, is recognized by Probe C.

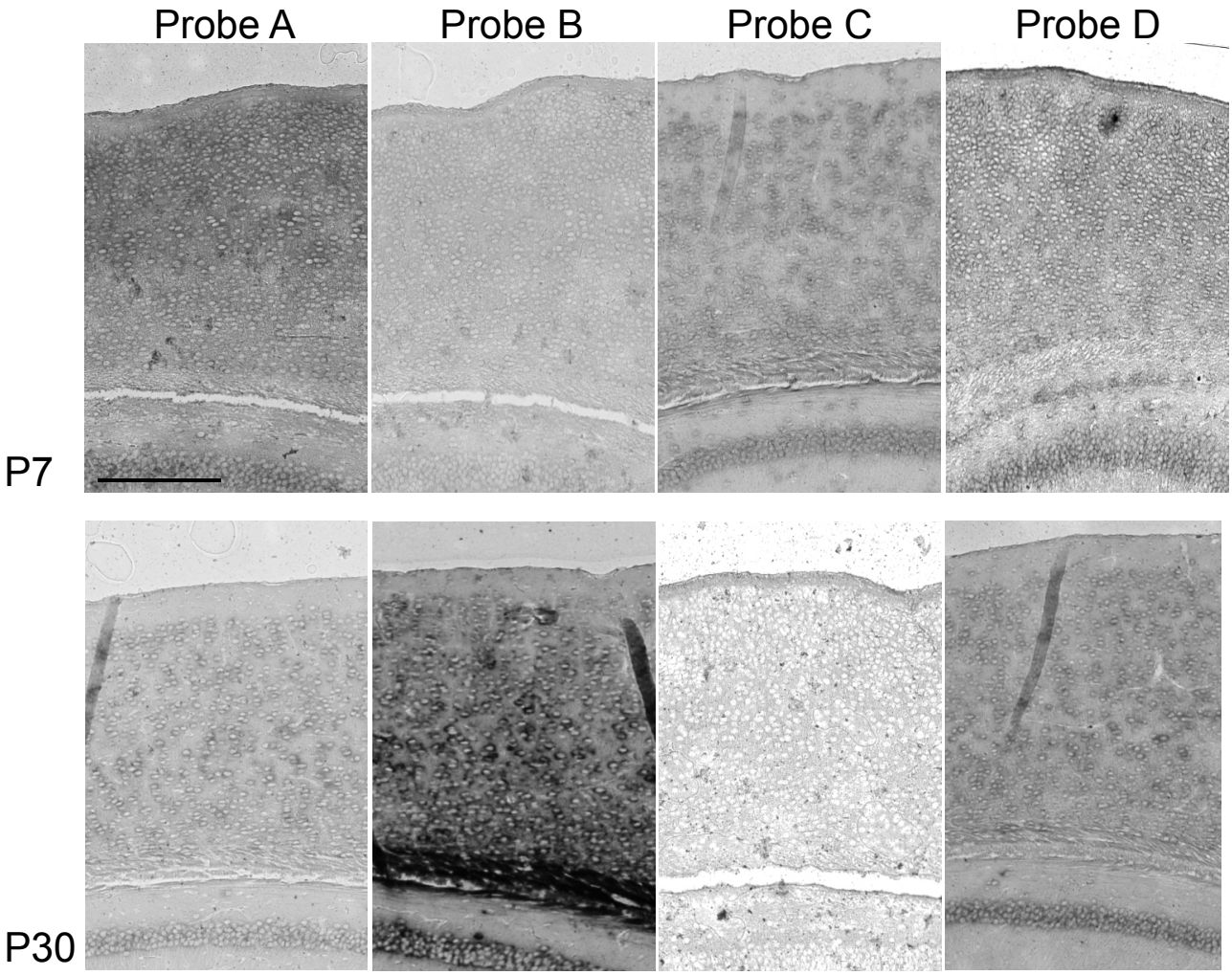

Figure 7. Different localization of the DCLK1 isoforms in the cortex.

In the cortex, at P7 a similar pattern of expression is visible in probes A and D, but no signal is detectable in probes C and D. At P30, the opposite effect is observed, with widespread robust signal in the entirety of the thickness of the cortical plate in probe B. Scale bar: 250 um.

PROBE A - E14

PROBE B - E14

PROBE C - E14

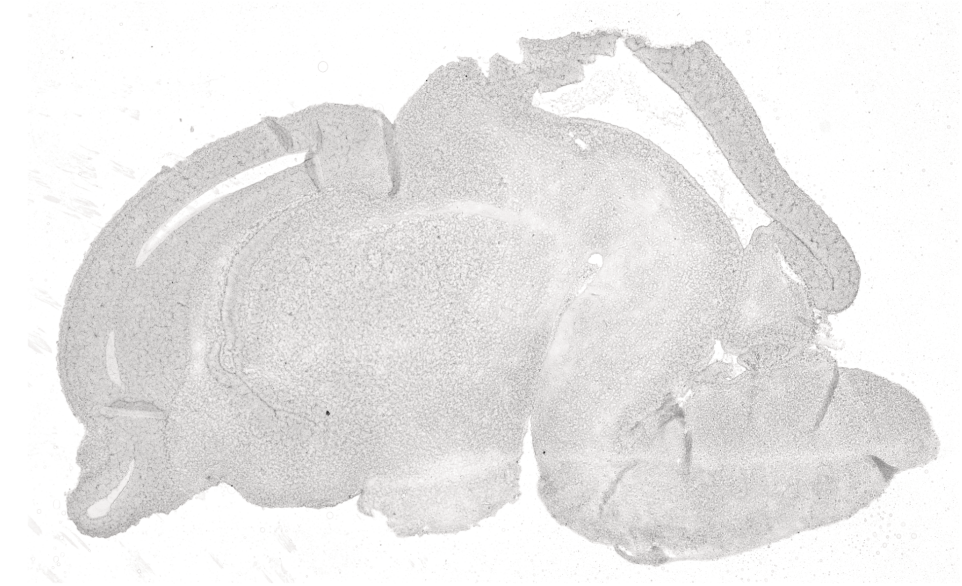

PROBE D - E14

PROBE A - P0

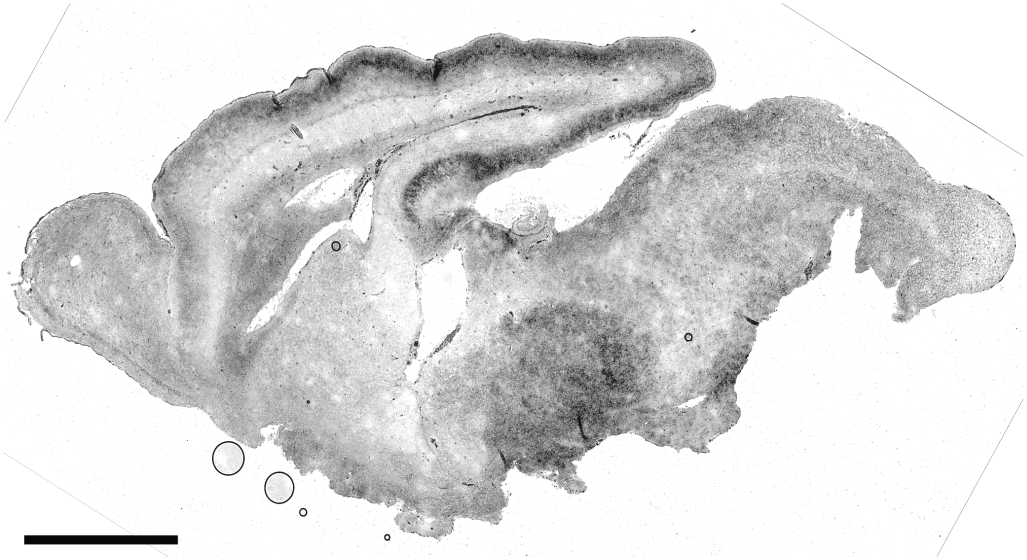

PROBE B - P0

PROBE C- P0

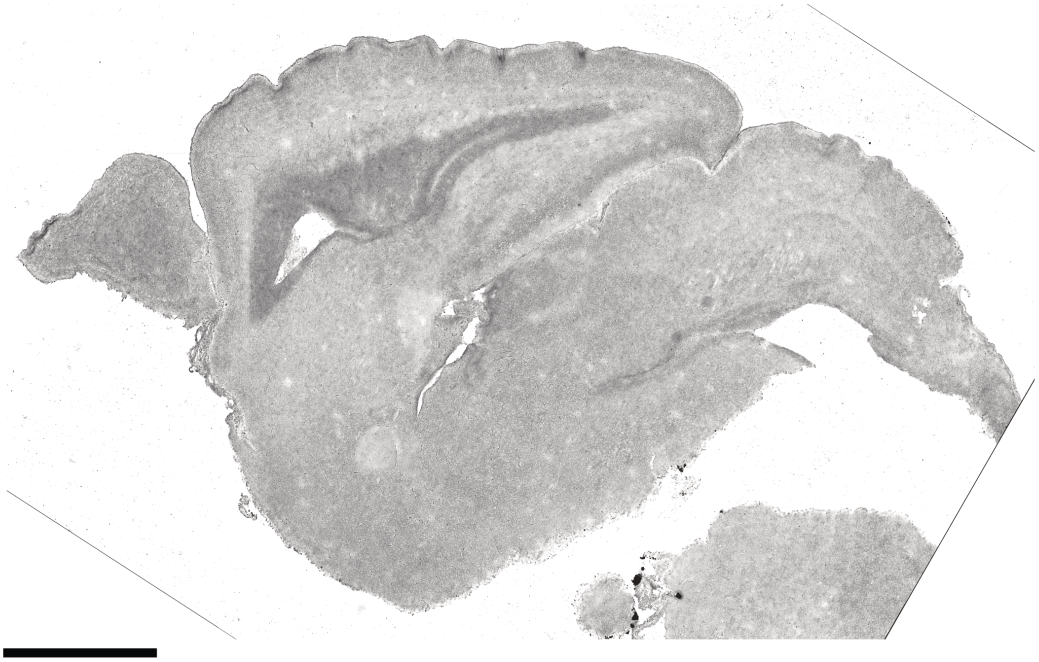

PROBE D - P0

PROBE A - P7

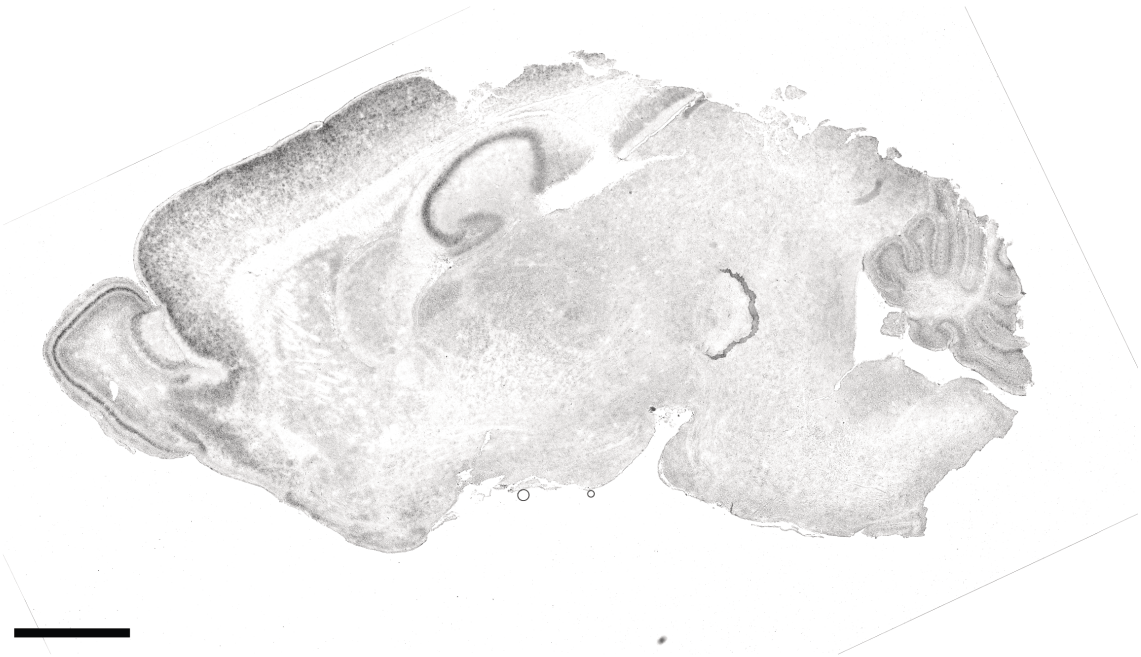

PROBE B - P7

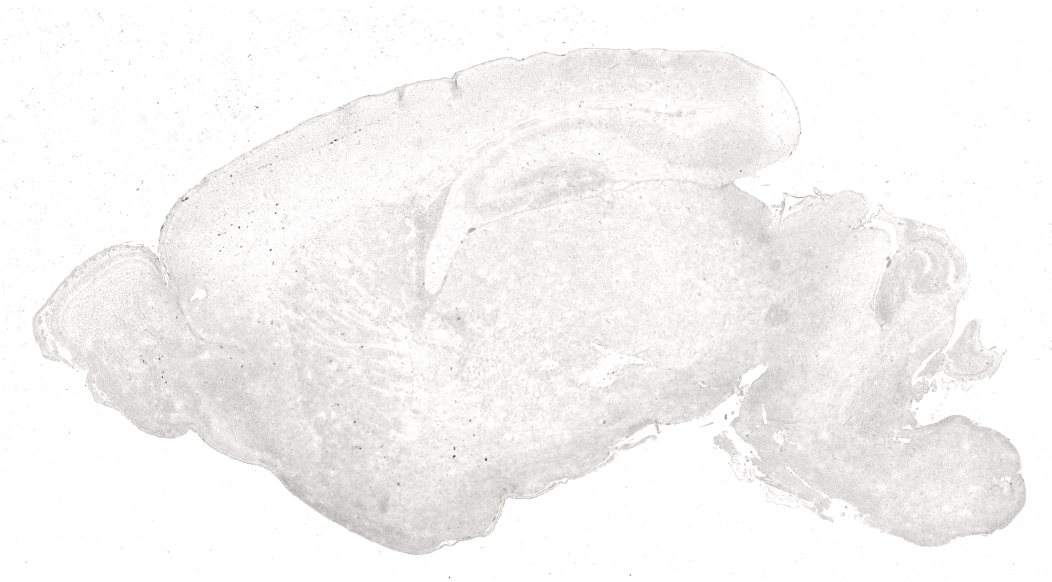

PROBE C - P7

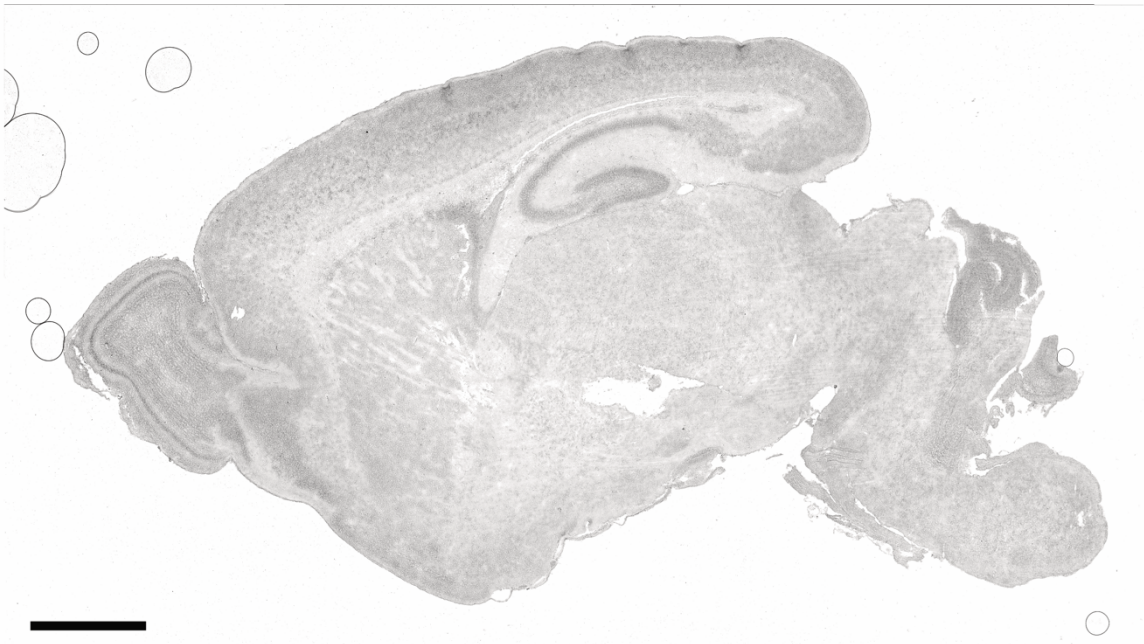

PROBE D - P7

PROBE A - P15

PROBE B - P15

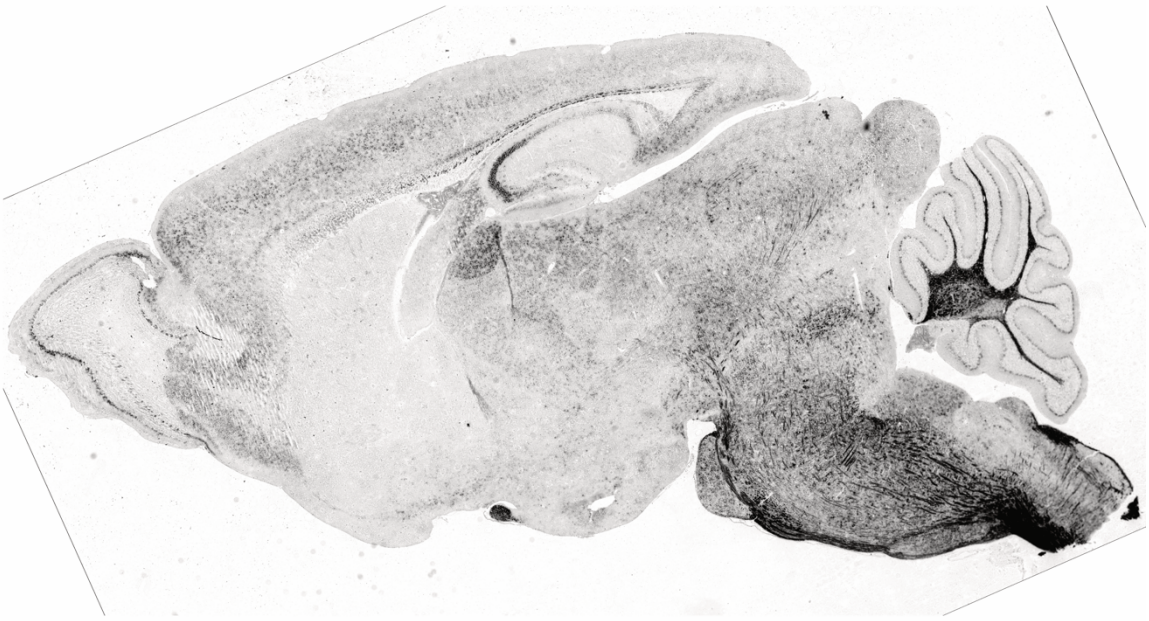

PROBE C - P15

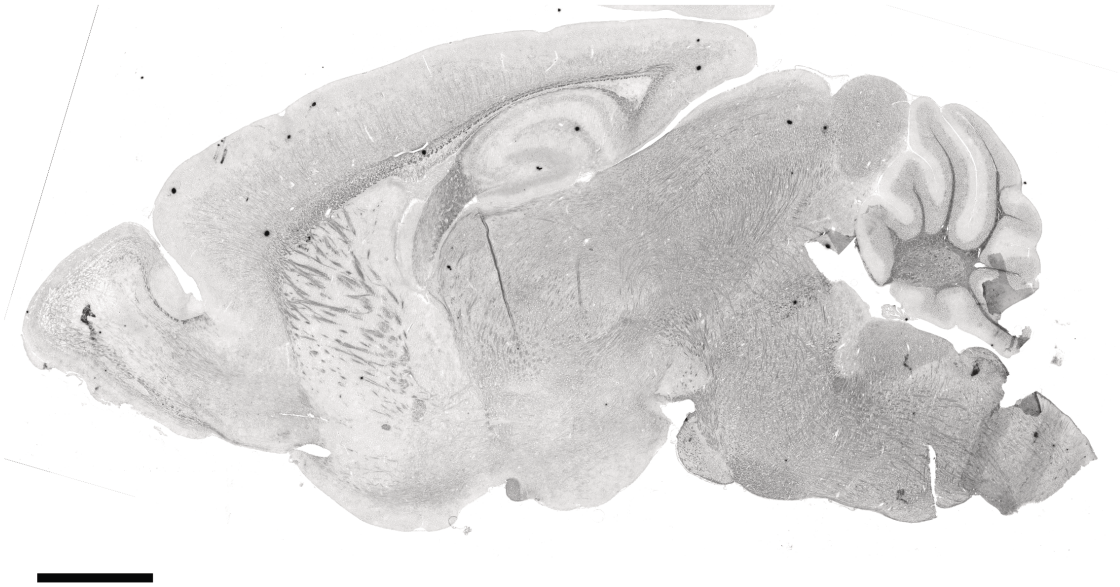

PROBE D - P15

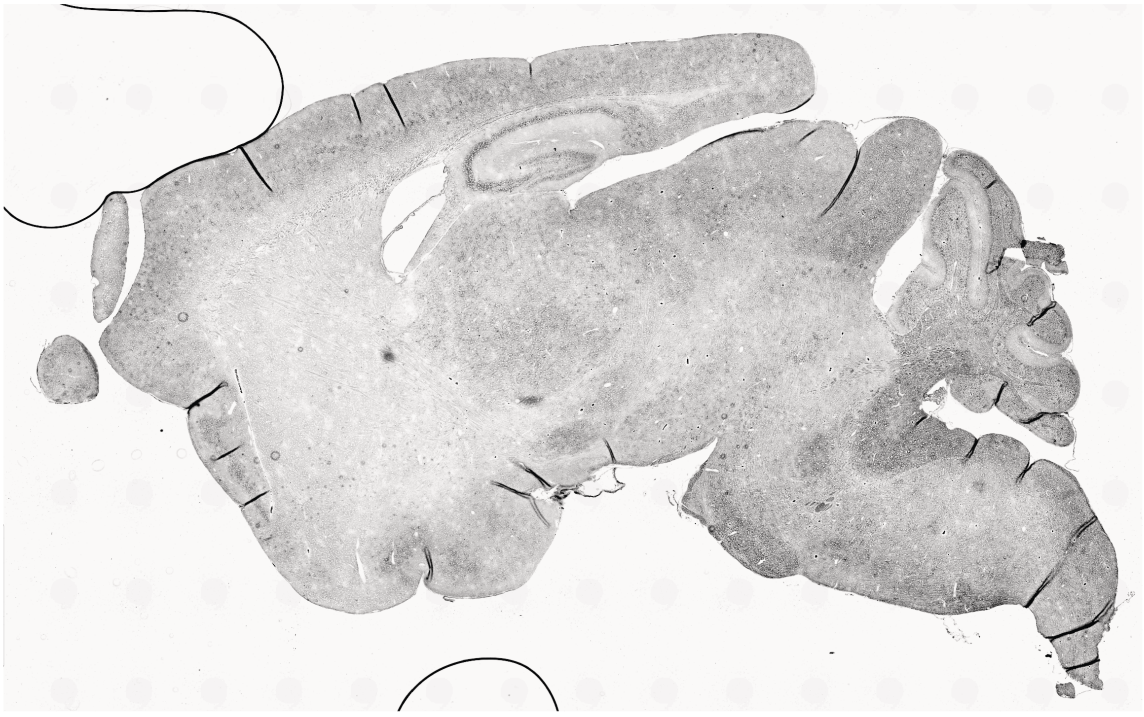

PROBE A - P30

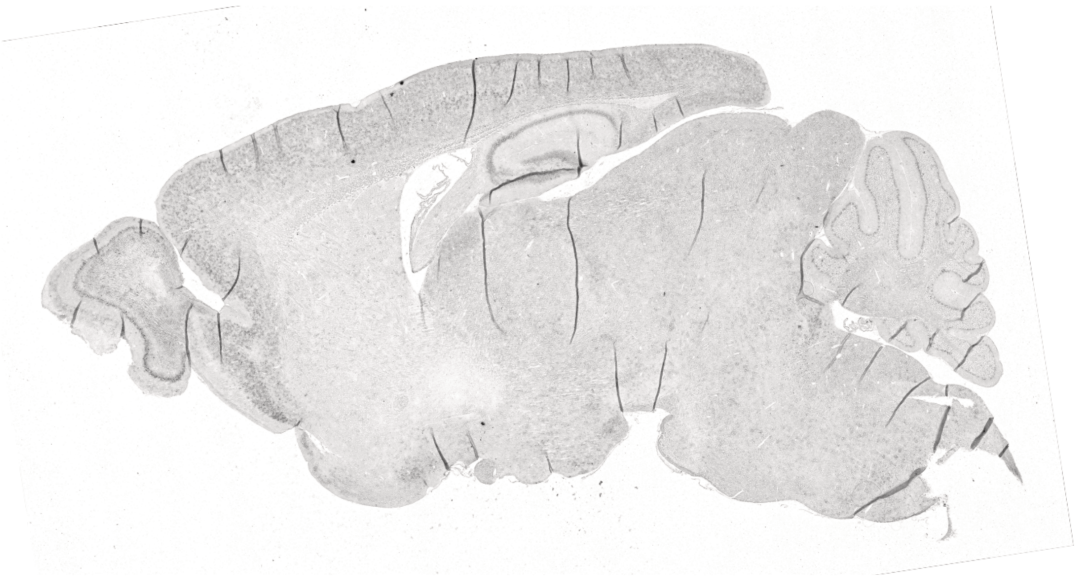

PROBE B - P30

PROBE C - P30

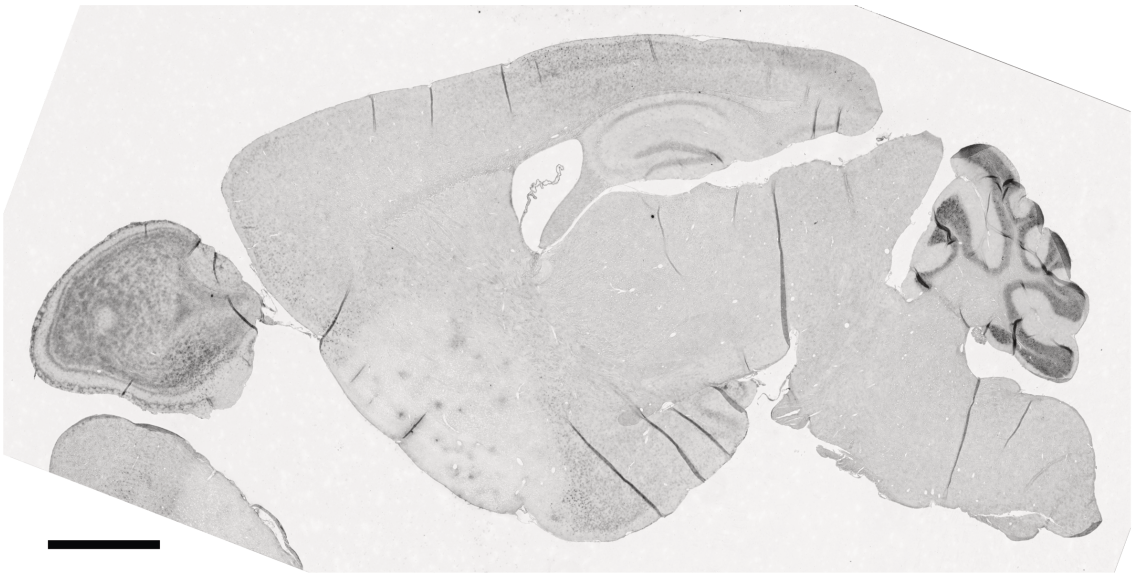

PROBE D - P30

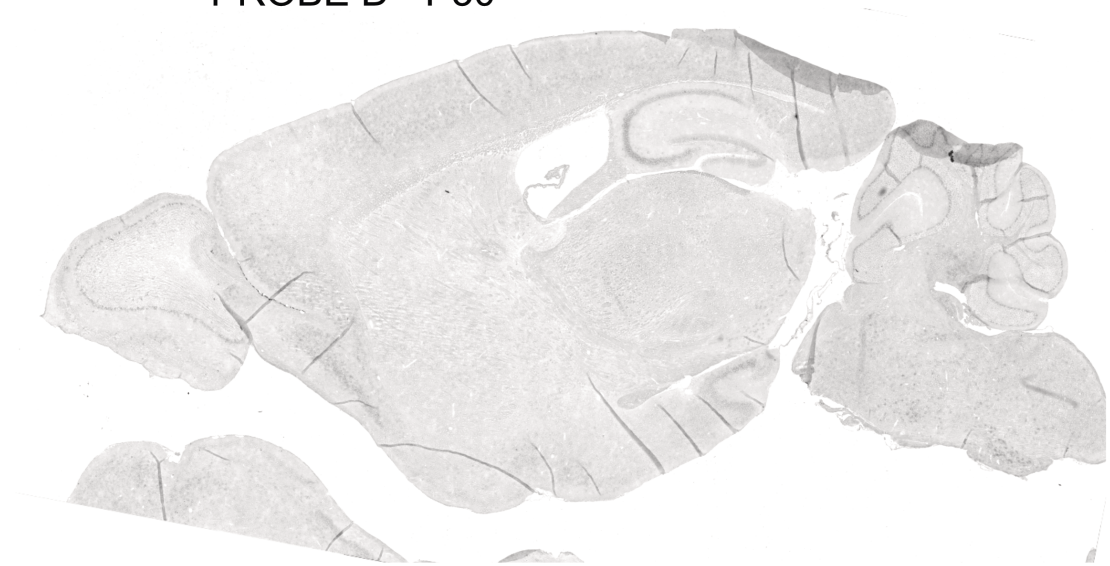

Figure 8. Whole brain expression pattern of the *Dclk1* mRNA in the developing brain. Comparison across different times points and probes highlights marked differences between samples. Scale bars: 1 mm.

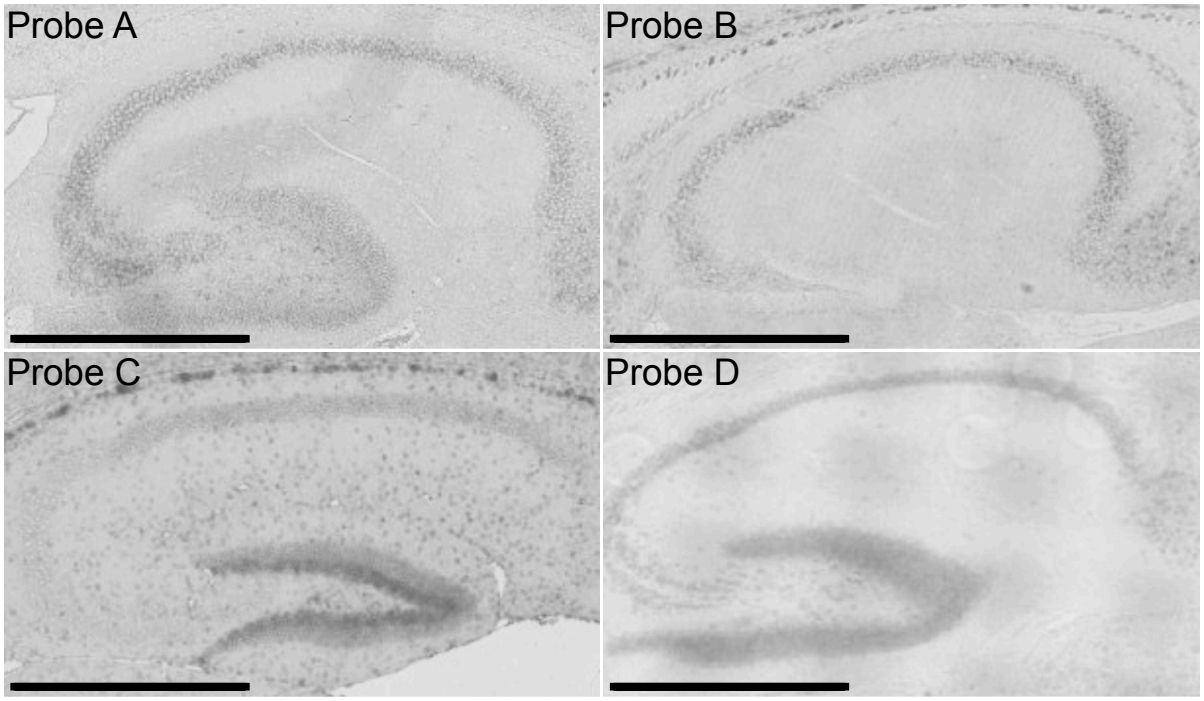

Figure 9. Differential expression in the hippocampus.

Higher magnification images of in situ hybridization in P30 hippocampus. The probes produce divergent region-specific patterns of signals. The lack of signal in Probe B in the DG suggests absence of CPG16 in that particular area. Scale bars: 500 um.

	CA1	CA3	DG
DCLK1-L	+	+	+
DCL	+	-	+
CPG16	+	+	-
CARP	?	?	-

Table 3. The isoforms segregate in different hippocampal regions.

Isoform expression and segregation can be inferred by comparing the ISH signal in the different probes. DCLK1-L is expressed in the entirety of the hippocampal formation, whereas DCL is expressed in the CA1 and DG, but not the CA3. The expression of CPG16, overlapping with DCLK1-L in the CA regions, is, on the other hand, absent in the DG. Finally, it was not possible to determine the expression of CARP. This could be due to a low or absent expression level of this variant at the stages observed.

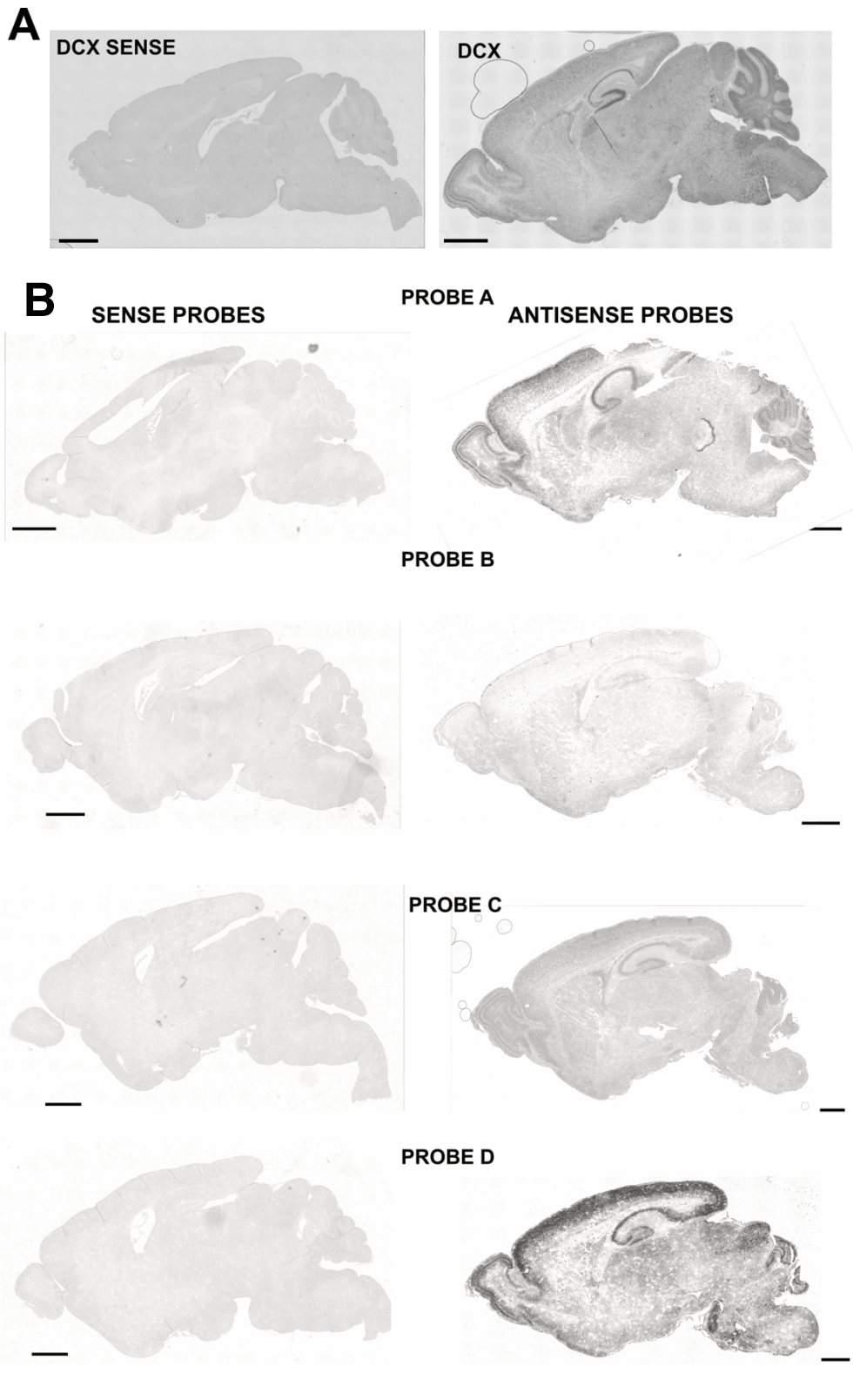
A
DCX SENSE
DCX
B
SENSE PROBES
PROBE A
ANTISENSE PROBES
PROBE B
PROBE C
PROBE D

Figure 10. ISH of DCX and sense probes show no detectable signal.

(A) DCX was used as a positive control, to confirm the experimental soundness of the ISH preparation. This protein was chosen because of its strong expression in newly generated neurons migrating radially and on the rostral migratory stream, as the figure, taken at P7, shows. The sense probe shows no signal. (B) Antisense and sense probes for the four probes comparison. The sense probes show no detectable signal, hence confirming that the signal seen experimentally is not background. Scale bars: 1 mm

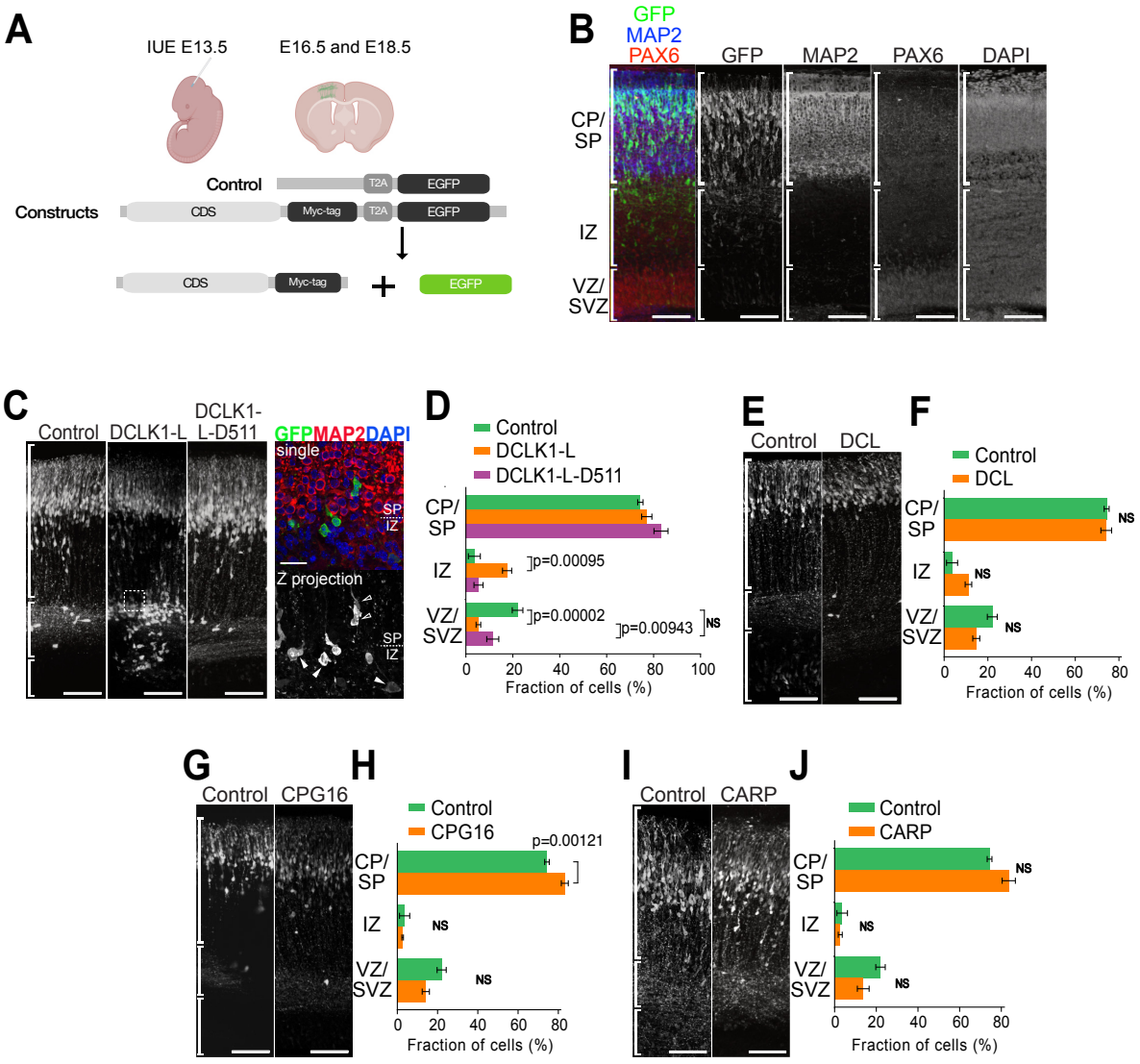
A
IUE E13.5
E16.5 and E18.5
Control
Constructs
CDS
T2A
EGFP
Myc-tag
B
GFP
MAP2
PAX6
DAPI
CP/
SP
IZ
VZ/
SVZ
C
Control
DCLK1-L
DCLK1-
L-D511
GFP MAP2 DAPI
single
SP
IZ
Z projection
D
Control
DCLK1-L
DCLK1-L-D511
p=0.00095
p=0.00002
p=0.00943
NS
Fraction of cells (%)
E
Control
DCL
F
Control
DCL
NS
G
Control
CPG16
H
Control
CPG16
p=0.00121
I
Control
CARP
J
Control
CARP

Figure 11. Effects of overexpression of DCLK1 isoforms in the developing mouse brain.
(A) Plasmids containing each variant tagged, T2A, and GFP were electroporated at E13.5 in the lateral ventricle. (B)) Representative image of a region of the cerebral cortex at E18, containing neurons electroporated at E13. Three zones of the cortical wall were defined by the immunolabeling of marker genes; the cortical plate and subplate (CP/SP) marked by MAP2, the intermediate zone (IZ) without staining of any markers, and the ventricular and subventricular zones (VZ/SVZ) labeled by PAX6. (C) At E18.5, DCLK1-L shows a significant number of cells stopping their radial migration in the IZ with a great ectopic accumulation. The dashed rectangle represents the higher magnification inset of (C). The neurons showing migration failure from the IZ of the mice receiving DCLK1-L overexpression demonstrate multipolar morphology (filled triangle). On the other hand, the neurons entered to the cortical plate demonstrate a bipolar morphology with a single leading process (open triangle). (D) Quantification shows a clear trend as a result from DCLK1-L overexpression, which is reversed in the kinase dead version. (E-J) No difference was found in DCL, CPG16 ,and CARP. Scale bar: 100 um (B, C, E, G, I); 25 um (inset in C). Data presented as mean ± SEM and p values ($p<0.01$) in one-way ANOVA, n=8.

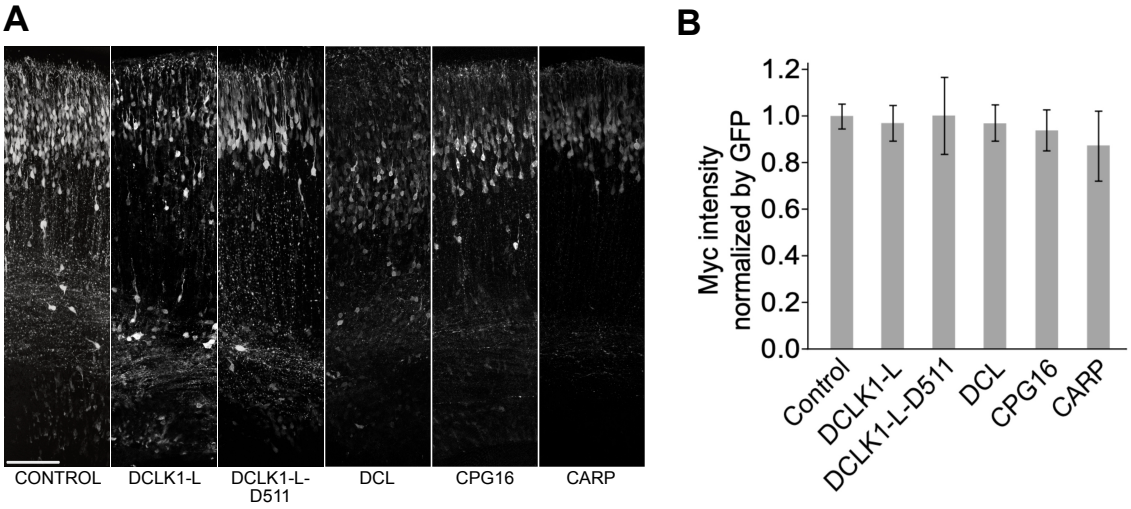

Figure 12. Quantification of fluorescence.

(A) Samples compared by quantifying the intensity of the Myc-tag antibody to avoid confounding effects in the IUE analysis which could arise from different protein expression levels. This is performed by first deconvoluting the raw images, thresholding them to remove the background, and then extracting the mean intensity of the objects in the raw pictures (in this case, fluorescent cells). I then repeated the procedure with GFP signal. To determine the relative intensity in the samples, I normalized the Myc stain intensity by GFP (B). This number is then further normalized to an average value and SD as previously described (Crowe and Yue, 2019). Scale bar: 100 um; Data are presented as mean ± SEM, and p values ($p<0.01$) in one-way ANOVA; n=8.

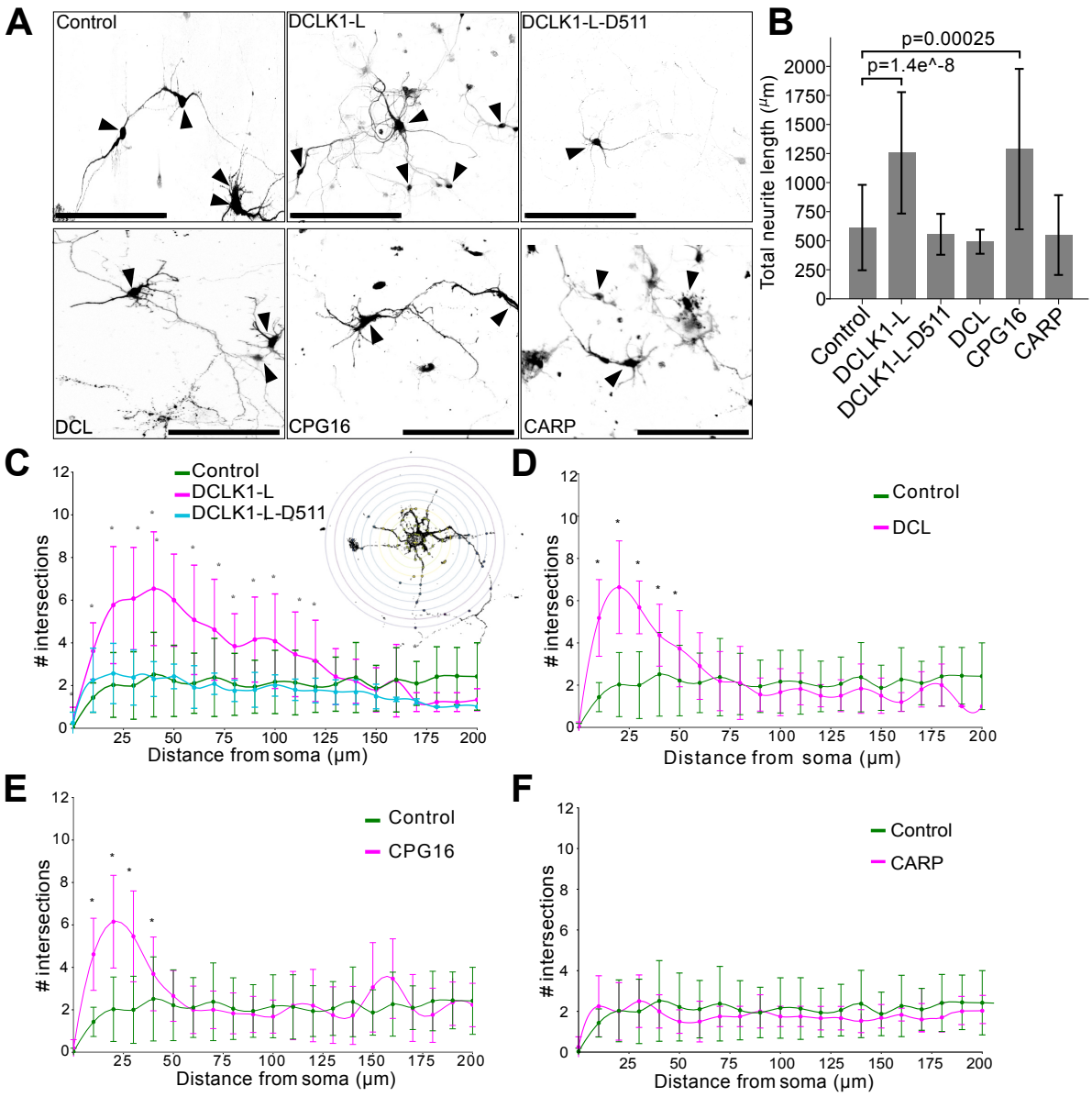
A
Control
DCLK1-L
DCLK1-L-D511
DCL
CPG16
CARP
B
p=0.00025
p=1.4e^-8
Total neurite length (μm)
2000
1750
1500
1250
1000
750
500
250
0
Control
DCLK1-L
DCLK1-L-D511
DCL
CPG16
CARP
C
Control
DCLK1-L
DCLK1-L-D511
intersections
Distance from soma (μm)
D
Control
DCL
intersections
Distance from soma (μm)
E
Control
CPG16
intersections
Distance from soma (μm)
F
Control
CARP
intersections
Distance from soma (μm)

Figure 13. Effects of overexpression of DCLK1 isoforms in dendrite development in cultured cortical neurons.

(A) Representative pictures of the different constructs' effects on dissociated cortical primary culture. (B) Comparison of the total neurite lengths across different variants. Overexpression of DCLK1-L and CPG16 show dramatic increase of dendritic growth. (C) Sholl analysis revealed that DCLK1-L gain-of-function shows the most obvious phenotype, which is completely reversed in the kinase-dead version. Sholl analysis is performed by centering the soma, and then drawing rings 10 um apart. The number of times neurites touch these rings (intersections) are counted and used in the plotting (inset in C). On the other hand, DCL (D), and CPG16 (E), show a less pronounced phenotype, with increased dendritic complexity present only proximally. CARP shows no difference with control construct (F). Data presented as mean ± SEM and p values ($p<0.01$) in one-way ANOVA. Number of cells analyzed: Control 340, DCLK1-L: 400; DCLK1-L-D511: 380; DCL: 280; CPG16: 380; CARP 380. Scale bar 100 um.

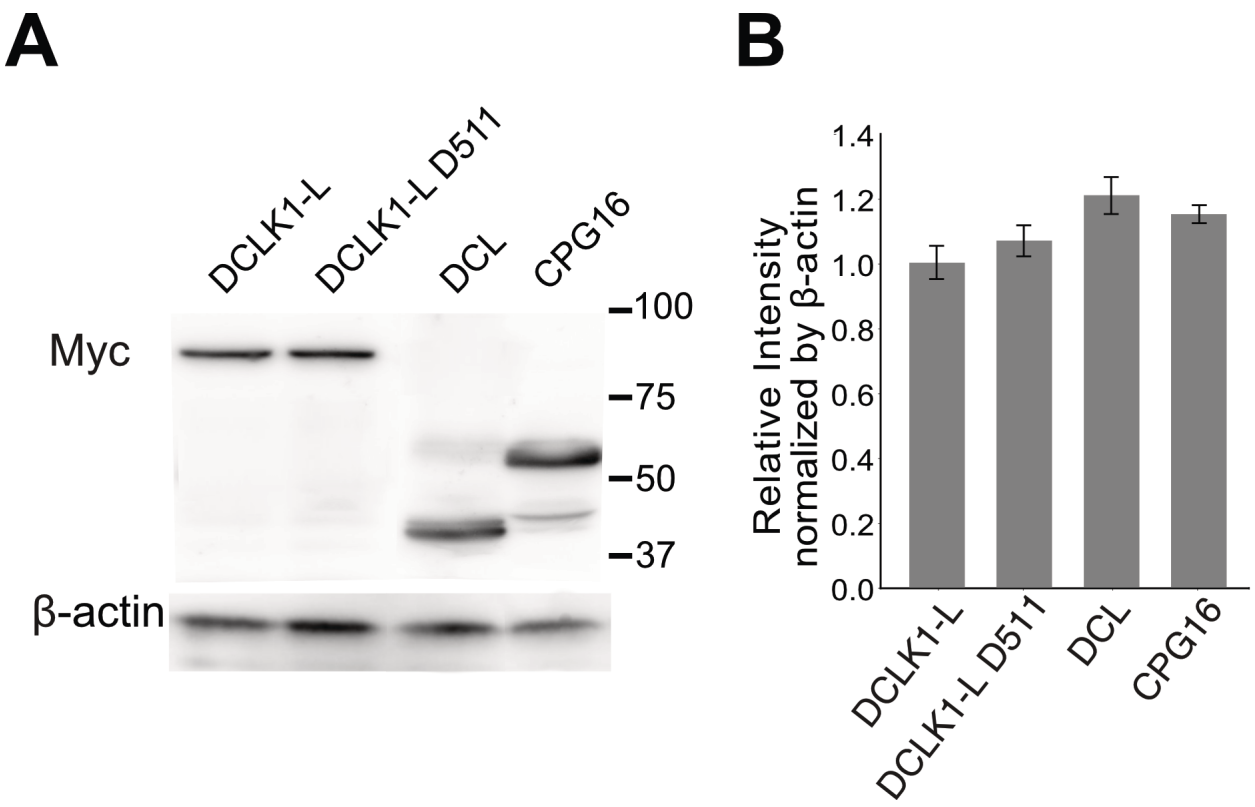

Figure 14. Expression vectors express DCLK1 proteins at the correct molecular weight and with similar relative abundance.

(A) Western Blot performed using the same constructs in HEK 293 cells confirmed both that the weight of the proteins was correct and the expression level of the constructs, which was comparable across samples. Stain was carried out with anti-Myc antibody with which the proteins were tagged. (B) To assess the expression level of the samples, relative intensity of constructs and actin loading control was extracted using FIJI, and then plotted using a custom Python script. Data presented as mean ± SEM and p values ($p<0.01$) in one-way ANOVA. N=3.

BIBLIOGRAPHY

Bauman, Tyler M, Emily A Ricke, Sally A Drew, Wei Huang, and William A Ricke (2016). "Quantitation of Protein Expression and Co-localization Using Multiplexed Immuno-histochemical Staining and Multispectral Imaging." eng. In: J Vis Exp 110. issn: 1940-087X (Electronic); 1940-087X (Linking). doi: 10.3791/53837.

Berke, J D, R F Paletzki, G J Aronson, S E Hyman, and C R Gerfen (1998). "A complex program of striatal gene expression induced by dopaminergic stimulation." eng. In: J Neurosci 18.14, pp. 5301–5310. issn: 0270-6474 (Print); 1529-2401 (Electronic); 0270-6474 (Linking). doi: 10.1523/JNEUROSCI. 18-14-05301.1998.

Bielas, Stephanie L, Finley F Serneo, Magdalena Chechlacz, Thomas J Deerinck, Guy A Perkins, Patrick B Allen, Mark H Ellisman, and Joseph G Gleeson (2007). "Spinophilin facilitates dephosphorylation of doublecortin by PP1 to mediate microtubule bundling at the axonal wrist." eng. In: Cell 129.3, pp. 579–591. issn: 0092-8674 (Print); 0092-8674 (Linking). doi: 10.1016/ j.cell.2007.03.023.

Binley, Kate E, Wai S Ng, James R Tribble, Bing Song, and James E Morgan (2014). "Sholl analysis: a quantitative comparison of semi-automated methods." eng. In: J Neurosci Methods 225, pp. 65–70. issn: 1872-678X (Elec- tronic); 0165-0270 (Linking). doi: 10.1016/j.jneumeth.2014.01.017.

Boekhoorn, Karin, Angela Sarabdjitsingh, Hendrik Kommerie, Karin de Punder, Theo Schouten, Paul J. Lucassen, and Erno Vreugdenhil (2008). "Doublecortin (DCX) and doublecortin-like (DCL) are differentially expressed in the early but not late stages of murine neocortical development." In: Journal of Comparative Neurology 507.4, pp. 1639–1652. doi: https://doi.org/ 10.1002/cne.21646. eprint: https://onlinelibrary.wiley.com/doi/ pdf/10.1002/cne.21646. url: https://onlinelibrary.wiley.com/ doi/abs/10.1002/cne.21646.

Braun, Martin, Robert Kirsten, Niels J Rupp, Holger Moch, Falko Fend, Nicolas Wernert, Glen Kristiansen, and Sven Perner (2013). "Quantification of protein expression in cells and cellular subcompartments on immunohistochemical sections using a computer supported image analysis system." eng. In: Histol Histopathol 28.5, pp. 605–610. issn: 1699-5848 (Electronic); 0213- 3911 (Linking). doi: 10.14670/HH-28.605.

Burgess, H A and O Reiner (2000). "Doublecortin-like kinase is associated with microtubules in neuronal growth cones." eng. In: Mol Cell Neurosci 16.5, pp. 529–541. issn: 1044-7431 (Print); 1044-7431 (Linking). doi: 10.1006/ mcne.2000.0891.

Burgess, Harold A. and Orly Reiner (2002). “Alternative Splice Variants of Doublecortin-like Kinase Are Differentially Expressed and Have Different Kinase Activities.” In: Journal of Biological Chemistry.

Chhatriya, Bishnupriya, Moumita Mukherjee, Sukanta Ray, Barsha Saha, Som- datta Lahiri, Sandip Halder, Indranil Ghosh, Sujan Khamrui, Kshaunish Das, Samsiddhi Bhattacharjee, Saroj Kant Mohapatra, and Srikanta Goswami (2020). “Transcriptome analysis identifies putative multi-gene signature distinguishing benign and malignant pancreatic head mass.” In: Journal of Translational Medicine 18.1, p. 420. doi: 10.1186/s12967-020-02597-1. url: https://doi.org/10.1186/s12967-020-02597-1.

Cooper, Jonathan A (2014). “Molecules and mechanisms that regulate multi- polar migration in the intermediate zone.” eng. In: Front Cell Neurosci 8, p. 386. issn: 1662-5102 (Print); 1662-5102 (Electronic); 1662-5102 (Link-ing). doi:10.3389/fncel.2014.00386.

Cregger, Melissa, Aaron J Berger, and David L Rimm (2006). “Immunohistochemistry and quantitative analysis of protein expression.” eng. In: Arch Pathol Lab Med 130.7, pp. 1026–1030. issn: 1543-2165 (Electronic); 0003- 9985 (Linking). doi: 10.1043/1543-2165(2006)130{$[$}1026:IAQAOP{$] $}2.0.CO;2.

Crowe, Alexandra R and Wei Yue (2019). “Semi-quantitative Determination of Protein Expression using Immunohistochemistry Staining and Analysis: An Integrated Protocol.” eng. In: Bio Protoc 9.24. issn: 2331-8325 (Print); 2331-8325 (Electronic); 2331-8325 (Linking). doi: 10.21769/BioProtoc. 3465.

Danielson, Nathan B, Patrick Kaifosh, Jeffrey D Zaremba, Matthew Lovett- Barron, Joseph Tsai, Christine A Denny, Elizabeth M Balough, Alexander R Goldberg, Liam J Drew, Ren´e Hen, Attila Losonczy, and Mazen A Kheirbek (2016). “Distinct Contribution of Adult-Born Hippocampal Granule Cells to Context Encoding.” eng. In: Neuron 90.1, pp. 101–112. issn: 1097-4199 (Electronic); 0896-6273 (Print); 0896-6273 (Linking). doi: 10.1016/j. neuron.2016.02.019.

Deuel TA, Liu JS, Corbo JC, Yoo SY, Rorke-Adams LB, Walsh CA. Genetic interactions between doublecortin and doublecortin-like kinase in neuronal migration and axon outgrowth. Neuron. 2006 Jan 5;49(1):41-53. doi: 10.1016/j.neuron.2005.10.038. PMID: 16387638.

Engels, Bart M, Theo G Schouten, Joost van Dullemen, Ilse Gosens, and Erno Vreugdenhil (2004). “Functional differences between two DCLK splice vari- ants.” eng. In: Brain Res Mol Brain Res 120.2, pp. 103–114. issn: 0169-328X (Print); 0169-328X (Linking). doi: 10.1016/j.molbrainres.2003.10.006.

Erno Vreugdenhil Nicole Datson, Bart Engels Jeannette de Jong Silvana van Koningsbruggen Marcel Schaaf E. Ronald de Kloet (1999). “Kainate-elicited seizures

induce mRNA encoding a CaMK-related peptide: A putative modulator of kinase activity in rat hippocampus." In:

Ferreira, Tiago A, Arne V Blackman, Julia Oyrer, Sriram Jayabal, Andrew J Chung, Alanna J Watt, P Jesper Sj¨ostr¨om, and Donald J van Meyel (2014). "Neuronal morphometry directly from bitmap images." eng. In: Nat Methods 11.10, pp. 982–984. issn: 1548-7105 (Electronic); 1548-7091 (Print); 1548- 7091 (Linking). doi: 10.1038/nmeth.3125.

Francis, F, A Koulakoff, D Boucher, P Chafey, B Schaar, M C Vinet, G Friocourt, N McDonnell, O Reiner, A Kahn, S K McConnell, Y Berwald-Netter, P Denoulet, and J Chelly (1999). "Doublecortin is a developmentally regulated, microtubule-associated protein expressed in migrating and differentiating neurons." eng. In: Neuron 23.2, pp. 247–256. issn: 0896-6273 (Print); 0896- 6273 (Linking). doi: 10.1016/s0896-6273(00)80777-1.

Garrido-Martin, Diego, Emilio Palumbo, Roderic Guig´o, and Alessandra Breschi (Aug. 2018). "ggsashimi: Sashimi plot revised for browser- and annotation- independent splicing visualization." In: PLOS Computational Biology 14.8, pp. 1–6. doi: 10.1371/journal.pcbi.1006360. url: https://doi. org/10.1371/journal.pcbi.1006360.

Gassmann, Max, Beat Grenacher, Bianca Rohde, and Johannes Vogel (2009). "Quantifying Western blots: Pitfalls of densitometry." In: ELECTROPHORE- SIS 30.11, pp. 1845–1855. doi: https://doi.org/10.1002/elps. 200800720. eprint: https://onlinelibrary.wiley.com/doi/pdf/10.002/elps.200800720. url: https://onlinelibrary.wiley.com/ doi/abs/10.1002/elps.200800720.

Gleeson, J G, K M Allen, J W Fox, E D Lamperti, S Berkovic, I Scheffer, E C Cooper, W B Dobyns, S R Minnerath, M E Ross, and C A Walsh (1998). "Doublecortin, a brain-specific gene mutated in human X-linked lissencephaly and double cortex syndrome, encodes a putative signaling pro- tein." eng. In: Cell 92.1, pp. 63–72. issn: 0092-8674 (Print); 0092-8674 (Linking). doi: 10.1016/s0092-8674(00)80899-5.

Gleeson, J G, P T Lin, L A Flanagan, and C A Walsh (1999). "Doublecortin is a microtubule-associated protein and is expressed widely by migrating neurons." eng. In: Neuron 23.2, pp. 257–271. issn: 0896-6273 (Print); 0896- 6273 (Linking). doi: 10.1016/s0896-6273(00)80778-3.

Gottesman, Irving I and Todd D Gould (2003). "The endophenotype concept in psychiatry: etymology and strategic intentions." eng. In: Am J Psychiatry 160.4, pp. 636–645. issn: 0002-953X (Print); 0002-953X (Linking). doi: 10.1176/appi.ajp.160.4.636.

Håvik, Bjarte, Franziska A. Degenhardt, Stefan Johansson, Carla P. D. Fernandes, Anke Hinney, Andre Scherag, Helle Lybæk, Srdjan Djurovic, Andrea Christoforou, Kari M. Ersland, Sudheer Giddaluru, Michael C. O'Donovan, Michael J. Owen, Nick

Craddock, Thomas W. Mu¨hleisen, Manuel Mattheisen, Benno G. Schimmelmann, Tobias Renner, Andreas Warnke, Beate Herpertz- Dahlmann, Judith Sinzig, Ozgur Albayrak, Marcella Rietschel, Markus M. Nothen, Clive R. Bramham, Thomas Werge, Johannes Hebebrand, Jan Haavik, Ole A. Andreassen, Sven Cichon, Vidar M. Steen, and Stephanie Le Hellard (Apr. 2012). “DCLK1 Variants Are Associated across Schizophrenia and At- tention Deficit/Hyperactivity Disorder.” In: PLOS ONE 7.4, pp. 1–12. doi:10.1371/journal.pone.0035424. url:https://doi.org/10.1371/journal.pone.0035424.

Hevroni, Dana, Amir Rattner, Marsha Bundman, Doron Lederfein, Awni Gabarah, Miriam Mangelus, Michael A. Silverman, Hilla Kedar, Cathy Naor, Masayo Kornuc, Tamar Hanoch, Rony Seger, Lars E. Theill, Elly Nedivi, Gal Richter- Levin, and Yoav Citri (1998). “Hippocampal plasticity involves extensive gene induction and multiple cellular mechanisms.” In: Journal of Molecular Neuroscience 10.2, pp. 75–98. doi: 10.1007/BF02737120. url: https: //doi.org/10.1007/BF02737120.

Kaiser, Odett, Pooyan Aliuos, Kirsten Wissel, Thomas Lenarz, Darja Werner, Gu¨nter Reuter, Andrej Kral, and Athanasia Warnecke (2013). “Dissociated neurons and glial cells derived from rat inferior colliculi after digestion with papain.” eng. In: PLoS One 8.12, e80490. issn: 1932-6203 (Electronic); 1932-6203 (Linking). doi: 10.1371/journal.pone.0080490.

Katz, Yarden, Eric T Wang, Edoardo M Airoldi, and Christopher B Burge (2010). “Analysis and design of RNA sequencing experiments for identifying isoform regulation.” In: Nature Methods 7.12, pp. 1009–1015. doi: 10.1038/nmeth.1528. url: https://doi.org/10.1038/nmeth.1528.

Kim, Daehwan, Joseph M. Paggi, Chanhee Park, Christopher Bennett, and Steven L. Salzberg (2019). “Graph-based genome alignment and genotyp- ing with HISAT2 and HISAT-genotype.” In: Nature Biotechnology 37.8, pp. 907–915. doi: 10.1038/s41587-019-0201-4. url: https://doi. org/10.1038/s41587-019-0201-4.

Koizumi, Hiroyuki, Teruyuki Tanaka, and Joseph G Gleeson (2006). “Doublecortin- like kinase functions with doublecortin to mediate fiber tract decussation and neuronal migration.” eng. In: Neuron 49.1, pp. 55–66. issn: 0896-6273 (Print); 0896-6273 (Linking). doi: 10.1016/j.neuron.2005.10.040.

Koizumi, Hiroyuki, Hiromi Fujioka, Kazuya Togashi, James Thompson, John R. Yates III, Joseph G. Gleeson, and Kazuo Emoto (2017). “DCLK1 phosphorylates the microtubule-associated protein MAP7D1 to promote axon elongation in cortical neurons.” In: Developmental Neurobiology 77.4, pp. 493– 510. doi: https://doi.org/10.1002/dneu.22428. eprint: https: //onlinelibrary.wiley.com/doi/pdf/10.1002/dneu.22428. url: https://onlinelibrary.wiley.com/doi/abs/10.1002/dneu.22428.

Kroon, Tim, Eline van Hugte, Lola van Linge, Huibert D. Mansvelder, and Rhiannon M. Meredith (2019). “Early postnatal development of pyramidal neurons across layers of the mouse medial prefrontal cortex.” In: Scientific Reports 9.1, p. 5037. doi: 10.1038/s41598-019-41661-9. url: https: //doi.org/10.1038/s41598-019-41661-9.

Le Hellard, Stéphanie, Bjarte Håvik, Thomas Espeseth, Harald Breilid, Roger Løvlie, Michelle Luciano, Alan J Gow, Sarah E Harris, John M Starr, Karin Wibrand, Astri J Lundervold, David J Porteous, Clive R Bramham, Ian J Deary, Ivar Reinvang, and Vidar M Steen (2009). “Variants in doublecortin- and calmodulin kinase like 1, a gene up-regulated by BDNF, are associ- ated with memory and general cognitive abilities.” eng. In: PLoS One 4.10, e7534. issn: 1932-6203 (Electronic); 1932-6203 (Linking). doi: 10.1371/ journal.pone.0007534.

Li, Heng (Sept. 2011). “A statistical framework for SNP calling, mutation discovery, association mapping and population genetical parameter estimation from sequencing data.” In: Bioinformatics 27.21, pp. 2987–2993. issn: 1367-4803. doi: 10.1093/bioinformatics/btr509. eprint: https: //academic.oup.com/bioinformatics/article-pdf/27/21/2987/ 577342/btr509.pdf. url: https://doi.org/10.1093/bioinformatics/ btr509.

Li Y, Shen M, Stockton ME, Zhao X. Hippocampal deficits in neurodevelopmental disorders. Neurobiol Learn Mem. 2019 Nov;165:106945. doi: 10.1016/j.nlm.2018.10.001. Epub 2018 Oct 12. PMID: 30321651; PMCID: PMC6461531.

Lin, Peter T., Joseph G. Gleeson, Joseph C. Corbo, Lisa Flanagan, and Christo- pher A. Walsh (2000). “DCAMKL1 Encodes a Protein Kinase with Homol- ogy to Doublecortin that Regulates Microtubule Polymerization.” In: Jour- nal of Neuroscience 20.24, pp. 9152–9161. issn: 0270-6474. doi: 10.1523/ JNEUROSCI.20-24-09152.2000. eprint: https://www.jneurosci.org/ content/20/24/9152.full.pdf. url: https://www.jneurosci.org/ content/20/24/9152.

Lipka, Joanna, Lukas C Kapitein, Jacek Jaworski, and Casper C Hoogenraad (2016). “Microtubule-binding protein doublecortin-like kinase 1 (DCLK1) guides kinesin-3-mediated cargo transport to dendrites.” eng. In: EMBO J 35.3, pp. 302–318. issn: 1460-2075 (Electronic); 0261-4189 (Print); 0261- 4189 (Linking). doi: 10.15252/embj.201592929.

Longair, Mark H., Dean A. Baker, and J. Douglas Armstrong (July 2011). “Simple Neurite Tracer: open source software for reconstruction, visualization and analysis of neuronal processes.” In: Bioinformatics 27.17, pp. 2453– 2454. issn: 1367-4803. doi: 10.1093/bioinformatics/btr390. eprint: https : / / academic . oup . com / bioinformatics / article - pdf / 27 / 17/2453/598305/btr390.pdf. url: https://doi.org/10.1093/ bioinformatics/btr390.

Longo, Patti A, Jennifer M Kavran, Min-Sung Kim, and Daniel J Leahy (2013). “Transient mammalian cell transfection with polyethylenimine (PEI).” eng. In: Methods Enzymol 529, pp. 227–240. issn: 1557-7988 (Electronic); 0076- 6879 (Print); 0076-6879 (Linking). doi: 10.1016/B978-0-12-418687- 3.00018-5.

Lopez-Bigas, Nuria, Benjamin Audit, Christos Ouzounis, Genıs Parra, and Roderic Guigo (2005). “Are splicing mutations the most frequent cause of hereditary disease?” eng. In: FEBS Lett 579.9, pp. 1900–1903. issn: 0014-5793 Print); 0014-5793 (Linking). doi: 10.1016/j.febslet.2005.02.047.

Matsuo, Tomohiko, Tatsuya Hattori, Akari Asaba, Naokazu Inoue, Nobuhiro Kanomata, Takefumi Kikusui, Reiko Kobayakawa, and Ko Kobayakawa (2015). “Genetic dissection of pheromone processing reveals main olfactory system- mediated social behaviors in mice.” eng. In: Proc Natl Acad Sci U S A 112.3, E311–20. issn: 1091-6490 (Electronic); 0027-8424 (Print); 0027- 8424 (Linking). doi: 10.1073/pnas.1416723112.

Nadarajah, B., Brunstrom, J. E., Grutzendler, J., Wong, R. O., Pearlman, A. L. 2001. Two modes of radial migration in early development of the cerebral cortex. Nat. Neurosci. 4, 143–150.

Nagamine, Tadashi, Sachiko Shimomura, Noriyuki Sueyoshi, and Isamu Kameshita (Jan. 2011). “Influence of Ser/Pro-rich domain and kinase domain of double cortin-like protein kinase on microtubule-binding activity.” In: The Journal of Biochemistry 149.5, pp. 619–627. issn: 0021-924X. doi: 10.1093/jb/ mvr013. eprint: https://academic.oup.com/jb/article-pdf/149/ 5/619/6443118/mvr013.pdf. url: https://doi.org/10.1093/jb/ mvr013.

Noctor, S. C., Martínez-Cerdeño, V., Ivic, L., Kriegstein, A. R. 2004. Cortical neurons arise in symmetric and asymmetric division zones and migrate through specific phases. Nat. Neurosci. 7, 136–144.

Omori, Y, M Suzuki, K Ozaki, Y Harada, Y Nakamura, E Takahashi, and T Fujiwara (1998). “Expression and chromosomal localization of KIAA0369, a putative kinase structurally related to Doublecortin.” eng. In: J Hum Genet 43.3, pp. 169–177. issn: 1434-5161 (Print); 1434-5161 (Linking). doi: 10. 1007/s100380050063.

Patel, Onisha, Weiwen Dai, Mareike Mentzel, Michael D W Griffin, Juliette Serindoux, Yoann Gay, Stefanie Fischer, Shoukat Sterle, Ashleigh Kropp, Christopher J Burns, Matthias Ernst, Michael Buchert, and Isabelle S Lucet (2016). “Biochemical and Structural Insights into Doublecortin-like Kinase Domain 1.” eng. In: Structure 24.9, pp. 1550–1561. issn: 1878-4186 (Elec- tronic); 0969-2126 (Linking). doi: 10.1016/j.str.2016.07.008.

Pike, Jeremy A, Iain B Styles, Joshua Z Rappoport, and John K Heath (2017). “Quantifying receptor trafficking and colocalization with confocal microscopy.” eng. In:

Methods 115, pp. 42–54. issn: 1095-9130 (Electronic); 1046-2023 (Linking). doi: 10.1016/j.ymeth.2017.01.005.

Portes, V des, F Francis, J M Pinard, I Desguerre, M L Moutard, I Snoeck, L C Meiners, F Capron, R Cusmai, S Ricci, J Motte, B Echenne, G Ponsot, O Dulac, J Chelly, and C Beldjord (1998). “doublecortin is the major gene causing X-linked subcortical laminar heterotopia (SCLH).” eng. In: Hum Mol Genet 7.7, pp. 1063–1070. issn: 0964-6906 (Print); 0964-6906 (Linking). doi: 10.1093/hmg/7.7.1063.

Rathi, Vinay K., Harlan M. Krumholz, Frederick A. Masoudi, and Joseph S. Ross (Aug. 2020). “Postmarket Clinical Evidence for High-Risk Therapeutic Med- ical Devices Receiving Food and Drug Administration Premarket Approval in 2010 and 2011.” In: JAMA Network Open 3.8, e2014496–e2014496. issn: 2574-3805. doi: 10.1001/jamanetworkopen.2020.14496. eprint: https: //jamanetwork.com/journals/jamanetworkopen/articlepdf/2769911/ rathi_2020_ld_200099_1602699681.74656.pdf. url: https: //doi.org/10.1001/jamanetworkopen.2020.14496.

Ristanović, Dušan, Nebojša T. Milšević, and Vesna Štulic (2006). “Application of modified Sholl analysis to neuronal dendritic arborization of the cat spinal cord.” In: Journal of Neuroscience Methods 158.2, pp. 212 –218. issn: 0165-0270. doi: https://doi.org/10.1016/j.jneumeth.2006.05. 030. url: http://www.sciencedirect.com/science/article/pii/ S0165027006002871.

Robinson, Mark D., Davis J. McCarthy, Gordon J. Smyth (2010). “edgeR: a Bioconductor package for differential expression analysis of digital gene expression data.” *Bioinformatics*, **26**(1), 139-140. doi: 10.1093/bioinformatics/btp616.

Saaltink, Dirk-Jan, Erik W van Zwet, and Erno Vreugdenhil (2020). “Doublecortin- Like Is Implicated in Adult Hippocampal Neurogenesis and in Motivational Aspects to Escape from an Aversive Environment in Male Mice.” eng. In: eNeuro 7.5. issn: 2373-2822 (Electronic); 2373-2822 (Linking). doi: 10. 1523/ENEURO.0324-19.2020.

Saaltink, Dirk-Jan, Bjarte H˚avik, Carla S Verissimo, P J Lucassen, and Erno Vreugdenhil (2012). “Doublecortin and doublecortin-like are expressed in overlapping and non-overlapping neuronal cell population: implications for neurogenesis.” eng. In: J Comp Neurol 520.13, pp. 2805–2823. issn: 1096- 9861 (Electronic); 0021-9967 (Linking). doi: 10.1002/cne.23144.

Schaar, Bruce T, Kazuhisa Kinoshita, and Susan K McConnell (2004). “Doublecortin microtubule affinity is regulated by a balance of kinase and phos- phatase activity at the leading edge of migrating neurons.” eng. In: Neu- ron 41.2, pp. 203–213. issn: 0896-6273 (Print); 0896-6273 (Linking). doi: 10.1016/s0896-6273(03)00843-2.

Schenk, Geert J, Bart Engels, Yan-Ping Zhang, Carlos P Fitzsimons, Theo Schouten, Marieke Kruidering, E Ron de Kloet, and Erno Vreugdenhil (2007). “A potential role for calcium / calmodulin-dependent protein kinase-related peptide in neuronal apoptosis: in vivo and in vitro evidence.” eng. In: Eur J Neurosci 26.12, pp. 3411–3420. issn: 1460-9568 (Electronic); 0953-816X (Linking). doi: 10.1111/j.1460-9568.2007.05956.x.

Schenk, Geert J, Barbera Veldhuisen, Olga Wedemeier, Caroline C McGown, Theo G Schouten, Melly Oitzl, E Ron de Kloet, and Erno Vreugdenhil (2010). “Over-expression of C-DCLK-short in mouse brain results in a more anxious behavioral phenotype.” eng. In: Physiol Behav 101.4, pp. 541– 548. issn: 1873-507X (Electronic); 0031-9384 (Linking). doi: 10.1016/ j.physbeh.2010.08.002.

Schenk, Geert J., Erno Vreugdenhil, Chantal J.Y. Hubens, Barbera Veldhuisen, E. Ron [de Kloet], and Melly S. Oitzl (2011). “Hippocampal CARP over- expression solidifies consolidation of contextual fear memories.” In: Phys- iology Behavior 102.3, pp. 323 – 331. issn: 0031-9384. doi: https : / / doi.org/10.1016/j.physbeh.2010.11.024. url: http://www. sciencedirect.com/science/article/pii/S0031938410004245.

Shin, Euikyung, Yutaro Kashiwagi, Toshihiko Kuriu, Hirohide Iwasaki, Teruyuki Tanaka, Hiroyuki Koizumi, Joseph G. Gleeson, and Shigeo Okabe (2013). “Doublecortin-like kinase enhances dendritic remodelling and negatively reg- ulates synapse maturation.” In: Nature Communications 4.1, p. 1440. doi: 10.1038/ncomms2443. url: https://doi.org/10.1038/ncomms2443.

Shu, Tianzhi, Huang-Chun Tseng, Tamar Sapir, Patrick Stern, Ying Zhou, Ka- mon Sanada, Andre Fischer, Fr´ed´eric M. Coquelle, Orly Reiner, and Li-Huei Tsai (2006). “Doublecortin-like Kinase Controls Neurogenesis by Regulat- ing Mitotic Spindles and M Phase Progression.” In: Neuron 49.1, pp. 25–39. doi: 10.1016/j.neuron.2005.10.039. url: https://doi.org/10. 1016/j.neuron.2005.10.039.

Silverman, M A, O Benard, H Jaaro, A Rattner, Y Citri, and R Seger (1999). “CPG16, a novel protein serine/threonine kinase downstream of cAMP- dependent protein kinase.” eng. In: J Biol Chem 274.5, pp. 2631–2636. issn: 0021-9258 (Print); 0021-9258 (Linking). doi: 10.1074/jbc.274.5.2631.

Soltesz, Ivan and Attila Losonczy (2018). “CA1 pyramidal cell diversity enabling parallel information processing in the hippocampus.” eng. In: Nat Neurosci 21.4, pp. 484–493. issn: 1546-1726 (Electronic); 1097-6256 (Print); 1097- 6256 (Linking). doi: 10.1038/s41593-018-0118-0.

Sossey-Alaoui, Khalid and Anand K. Srivastava (1999). “DCAMKL1, a Brain- Specific Transmembrane Protein on 13q12.3 That Is Similar to Doublecortin (DCX).” In: Genomics 56.1, pp. 121 –126. issn: 0888-7543. doi: https:// doi.org/10.1006/geno.1998.5718. url: http://www.sciencedirect. com/science/article/pii/S0888754398957184.

Tabata, H and K Nakajima (2001). “Efficient in utero gene transfer system to the developing mouse brain using electroporation: visualization of neuronal migration in the developing cortex.” eng. In: Neuroscience 103.4, pp. 865– 872. issn: 0306-4522 (Print); 0306-4522 (Linking). doi: 10.1016/s0306- 4522(01)00016-1.

Tabata, Hidenori and Kazunori Nakajima (2003). “Multipolar migration: the third mode of radial neuronal migration in the developing cerebral cortex.” eng. In: J Neurosci 23.31, pp. 9996–10001. issn: 1529-2401 (Electronic); 0270-6474 (Print); 0270-6474 (Linking). doi: 10.1523/JNEUROSCI.23- 31-09996.2003.

Tan, Han Yen and Tuck Wah Ng (2008). “Accurate step wedge calibration for densitometry of electrophoresis gels.” In: Optics Communications 281.10, pp. 3013 – 3017. issn: 0030-4018. doi: https://doi.org/10.1016/ j.optcom.2008.01.012. url: http://www.sciencedirect.com/ science/article/pii/S0030401808000461.

Tanaka, Teruyuki, Hiroyuki Koizumi, and Joseph G. Gleeson (July 2006). “The Doublecortin and Doublecortin-Like Kinase 1 Genes Cooperate in Murine Hippocampal Development.” In: Cerebral Cortex 16.suppl1, pp. i69–i73. issn: 1047-3211. doi: 10.1093/cercor/bhk005. eprint: https:// academic . oup . com / cercor / article - pdf / 16 / suppl \ _1 / i69 / 17295647/bhk005.pdf. url: https://doi.org/10.1093/cercor/bhk005.

Taylor, C R and R M Levenson (2006). “Quantification of immunohistochemistry–issues concerning methods, utility and semiquantitative assessment II.” eng.In: Histopathology 49.4, pp. 411–424. issn: 0309-0167 (Print); 0309-0167 (Linking). doi: 10.1111/j.1365-2559.2006.02513.x.

Vázquez-Vélez, Gabriel E, Kristyn A Gonzales, Jean-Pierre Revelli, Carolyn J Adamski, Fatemeh Alavi Naini, Aleksandar Baji´c, Evelyn Craigen, Ronald Richman, Sabrina M Heman-Ackah, Matthew J A Wood, Maxime W C Rousseaux, and Huda Y Zoghbi (2020). “Doublecortin-like Kinase 1 Regu- lates -Synuclein Levels and Toxicity.” eng. In: J Neurosci 40.2, pp. 459–477. issn: 1529-2401 (Electronic); 0270-6474 (Print); 0270-6474 (Linking). doi: 10.1523/JNEUROSCI.1076-19.2019.

Vreugdenhil E, Datson N, Engels B, de Jong J, van Koningsbruggen S, Schaaf M, de Kloet ER. Kainate-elicited seizures induce mRNA encoding a CaMK-related peptide: a putative modulator of kinase activity in rat hippocampus. J Neurobiol. 1999 Apr;39(1):41-50. PMID: 10213452.

Vreugdenhil, Erno, Sharon M. Kolk, Karin Boekhoorn, Carlos P. Fitzsimons, Marcel Schaaf, Theo Schouten, Angela Sarabdjitsingh, Rosana Sibug, and Paul J. Lucassen (2007). “Doublecortin-like, a microtubule-associated pro- tein expressed in radial glia, is crucial for neuronal precursor division and ra- dial process stability.” In: European Journal of Neuroscience 25.3, pp. 635– 648. doi: 10.1111/j.1460-9568.2007.05318.x.

eprint: https: //onlinelibrary.wiley.com/doi/pdf/10.1111/j.1460-9568. 2007.05318.x. url: https://onlinelibrary.wiley.com/doi/abs/ 10.1111/j.1460-9568.2007.05318.x.

Walsh, Thomas A.S. Deuel Judy S. Liu Joseph C. Corbo Seung-Yun Yoo Lucy B. Rorke-Adams Christopher A. (2006). “Genetic Interactions between Dou- blecortin and Doublecortin-like Kinase in Neuronal Migration and Axon Out- growth.” In:

Wu, Jing Qin, Xi Wang, Natalie J Beveridge, Paul A Tooney, Rodney J Scott, Vaughan J Carr, and Murray J Cairns (2012). “Transcriptome sequenc- ing revealed significant alteration of cortical promoter usage and splicing in schizophrenia.” eng. In: PLoS One 7.4, e36351. issn: 1932-6203 (Elec- tronic); 1932-6203 (Linking). doi: 10.1371/journal.pone.0036351.

Yan, Qinghong, Sebastien M. Weyn-Vanhentenryck, Jie Wu, Steven A. Sloan, Ye Zhang, Kenian Chen, Jia Qian Wu, Ben A. Barres, and Chaolin Zhang (2015). “Systematic discovery of regulated and conserved alternative exons in the mammalian brain reveals NMD modulating chromatin regulators.” In: Proceedings of the National Academy of Sciences 112.11, pp. 3445– 3450. issn: 0027-8424. doi: 10.1073/pnas.1502849112. eprint: https: //www.pnas.org/content/112/11/3445.full.pdf. url: https: //www.pnas.org/content/112/11/3445.

Zygmunt, Magdalena, Dz˙esika Hoinkis, Jacek Hajto, Marcin Piechota, Boz˙ena Skupien´-Rabian, Urszula Jankowska, Sylwia Kedracka-Krok, Jan Rodriguez Parkitna,andMichal□Korostyn´ski(2018).“Expressionofalternativelyspliced variants of the Dclk1 gene is regulated by psychotropic drugs.” eng. In: BMC Neurosci 19.1, p. 55. issn: 1471-2202 (Electronic); 1471-2202 (Linking). doi: 10.1186/s12868-018-0458-4.